https://doi.org/10.5194/egusphere-2023-267
Preprint. Discussion started: 6 March 2023

Dynamic savanna burning emission factors based on satellite data using a machine learning approach

Roland Vernooij[1], Tom Eames[1], Jeremy Russel-Smith[2,3], Cameron Yates[2,3], Robin Beatty[3,4], Jay Evans[2,3], Andrew Edwards[2,3], Natasha Ribeiro[5], Martin Wooster[6,7], Tercia Strydom[8], Marcos Vinicius Giongo Alves[9], Marco Assis Borges[10], Máximo Menezes Costa[10], Ana Carolina Sena Barradas[10], Dave van Wees[1], Guido R. Van der Werf[1]

[1]Department of Earth Sciences, Faculty of Science, Vrije Universiteit Amsterdam, Amsterdam, The Netherlands
[2]Darwin Centre for Bushfire Research, Charles Darwin University, Darwin, 0909, Northern Territory, Australia
[3]International Savanna Fire Management Initiative (ISFMI), New South Wales, Australia
[4] 321Fire, Lda, Inhambane, Mozambique
[5]Faculty of Agronomy and Forest Engineering, Eduardo Mondlane University, Maputo, Mozambique
[6]King's College London, Environmental Monitoring and Modelling Research Group, Department of Geography, UK
[7]National Centre for Earth Observation (NERC), UK
[8]South African National Parks (SANParks), Kruger National Park, South Africa
[9]Center for Environmental Monitoring and Fire Management (CEMAF), Federal University of Tocantins, Gurupi, Brazil
[10]Chico Mendes institute for Conservation of Biodiversity (ICMBio), Rio da Conceição, Brazil

Correspondence to: Roland Vernooij (r.vernooij@vu.nl)

Abstract. Landscape fires, predominantly in the frequently burning global savannas, are a substantial source of greenhouse gases and aerosols. The impact of these fires on atmospheric composition is partially determined by the chemical breakup of the elements in the fuel into individual emitted chemical species, which is described by emission factors (EFs). These EFs are known to be dependent on, amongst others, the type of fuel consumed, the moisture content of that fuel and the meteorological conditions during the fire, indicating that savanna EFs are temporally and spatially dynamic. Global emission inventories, however, rely on static biome-averaged EFs which makes them ill-suited for the estimation of regional biomass burning (BB) emissions and for capturing the effects of shifts in fire regimes. In this study we explore the main drivers of EF-variability within the savanna biome and assess which geospatial proxies can be used to estimate dynamic EFs for global models. We collected over 4500 EF bag measurements of CO_2, CO, CH_4 and N_2O using an unmanned aerial system (UAS), and measured fuel parameters and fire severity proxies during 129 individual fires. The measurements cover a variety of savanna ecosystems under different seasonal conditions, sampled over the course of six fire seasons between 2017 and 2022. We complemented our own data with EFs from 85 fires with known locations and dates listed in the literature. Based on the locations, dates and time of the fires we retrieved a variety of fuel-, weather- and fire severity proxies (i.e. possible predictors) using globally available satellite and reanalysis data. We then trained random forest (RF) regressors to estimate dynamic EFs for CO_2, CO, CH_4 and N_2O and calculated the spatiotemporal impact on BB emissions over the 2002–2016 period using the Global Fire Emissions Database version 4 with small fires (GFED4s). We found that the most important field indicators for the EFs of CO_2, CO and CH_4 were tree cover density, fuel moisture content and the grass to litter ratio. The grass to litter ratio and the nitrogen to carbon ratio were important indicators for N_2O EFs. RF models using satellite observations performed well for the prediction of EF variability in the measured fires with out-of-sample correlation coefficients between

0.80 and 0.99, reducing the error in EF estimates by 60–85% compared to static biome averages. Using dynamic EFs, global savanna emission estimates for 2002–2016 were 1.8% higher for CO while CH_4 and N_2O emissions were respectively 5% and 18% lower compared to GFED4s. On a regional scale we found a spatial redistribution compared to GFED4s with higher CO, CH_4 and N_2O EFs in mesic regions and lower ones in xeric regions. Seasonal drying resulted in a decrease of the EFs of these species with the fire season progressing, with a stronger trend in open savannas than woodlands. Contrary to the minor impact on annual savanna average emissions, the model predicts localized reductions in EFs of CO, CH_4 and N_2O exceeding 60% under seasonal conditions.

1 Introduction

Landscape fires emit substantial amounts of gases, including the greenhouse gases CO_2, CH_4, and N_2O which affect the Earth's climate. To quantify the impact of these fire emissions, and track the role of fire in the biogeochemical system, fire emission inventories like the Global Fire Emissions Database (GFED, van der Werf et al., 2017) and the Global Fire Assimilation System (GFAS, Kaiser et al., 2012) use satellite observations to monitor global landscape fires. They estimate that, due to their high burning frequency, savannas account for roughly 60% of the global carbon emissions from biomass burning (BB). The impact of fire emissions on atmospheric radiative forcing is strongly dependent on the partitioning of burned biomass into individual emission species, which in part depends on the combustion efficiency (often simplified as the CO_2 emissions divided by the combined CO_2 and CO emissions, referred to as the modified combustion efficiency or MCE) during the fire. For this partitioning, models currently use biome-specific emission factors (EFs), expressed in grams of a molecule emitted for each kilogram of dry matter (DM) burned. However, measurements from both laboratory and landscape fires indicate that important drivers of fire intensity and combustion efficiency, e.g. the moisture content of the fuel (Chen et al., 2010) and the curing state of grasses (Korontzi et al., 2003b), are seasonal and that therefore EFs are both spatially and temporally dynamic.

Field measurements of BB EFs have been inventoried for a large number of chemical species (Akagi et al., 2011; Andreae, 2019) and also indicate substantial intra-biome variability. Due to the lack of direct field measurements and their limited geospatial and temporal coverage, the variability in EFs has been difficult to quantify for the incorporation in global models (van Leeuwen and van der Werf, 2011). This makes current global models ill-equipped to estimate emissions on local to regional scales. This results, for example, in the same EFs being assumed for a closed-canopy savanna woodland and an open grassland. Using historic averages also means that EFs do not dynamically change while fire regimes and environmental burning conditions can shift as a result of climate change or human interaction. One additional field of research that requires a better understanding of spatiotemporal dynamics involves fire management strategies in savannas to reduce fire emissions, with the aim of mitigating climate change. Over the past decennium, significant efforts have been directed at shifting the temporal patterns of savanna fire regimes in order to make them more sustainable and abate greenhouse gas emissions (e.g. Russell-Smith et al., 2013; Schmidt et al., 2018). EFs used for the accreditation of such projects currently assume a dichotomy of early- and late dry season averages, determined by a cut-off date. However, the fuel and meteorological conditions thought to drive EFs vary more gradually over the season and are moreover

https://doi.org/10.5194/egusphere-2023-267
Preprint. Discussion started: 6 March 2023

subjected to substantial inter-annual and spatial variability. Incorporating spatiotemporal variability in models therefore makes these models more dynamic and better equipped for assessing seasonal fluctuations.

Over the past six years (2017-2022), a series of savanna burning campaigns measuring EF measurements using unmanned aerial systems (UAS) have resulted in a large number of new measurements with broad spatiotemporal coverage (e.g. Vernooij et al., 2021, 2022; Russell-Smith et al., 2021). In this study we describe the variability identified in over 4500 individual bag samples of CO_2, CO, CH_4 and N_2O EFs covering 129 fires. Combined with the EFs from fires already reported in literature, these new EF measurements allow us to analyse the variability in BB EFs in more detail by using unexplored non-linear statistical methods like decision-tree-based machine learning algorithms. The non-linear nature of these models makes them suitable to quantify distinctive dynamics under different circumstances due to complex natural processes in landscape fires. This approach does require large datasets for training and validation which were not available until now. We first determine the dominant drivers of EF variability based on field measurements and then apply random forest regression methods to estimate dynamic EFs for the abovementioned species using globally available satellite data and geospatial reanalysis data. Depending on the application, these dynamic EFs can be computed at various spatiotemporal resolutions, limited by the resolution of the underlying features (i.e. starting from 500-meter and with hourly timesteps). Finally, we use GFED4s, in combination with the dynamic EFs –computed on a monthly basis at 0.25°– to estimate the emission dynamics over the 2002-2016 period.

2 Methods

The main objectives of this study are: (1) to identify the drivers of EF variability in the savanna biome and (2) to implement this variability into global models through dynamic EFs. The first objective requires a large dataset of EFs and a thorough assessment of a wide range of possible drivers, including direct field measurements of vegetation composition, meteorological conditions and fire intensity dynamics. This is described in section 2.1. The second objective requires a more globalized approach which allows BB EFs to be predicted based on satellite and reanalysis data with broad spatiotemporal coverage, see sections 2.2 and 2.3.

2.1 Field measurements

2.1.1 Measurement setup

Using a UAS-mounted sampling system we measured BB EFs of CO_2, CO, CH_4 and N_2O in fresh smoke during landscape fires, following the methodology described by Vernooij et al. (2021, 2022). Emissions were sampled at an altitude of between 5–50 m depending on flame height for a duration of 35 seconds, resulting in 0.7 litres of gas sample. Within 12 hours, these samples were measured using cavity-ringdown spectroscopy for atmospheric mixing ratios of CO_2 and CH_4 (Los Gatos Research, Microportable gas analyser), and CO and N_2O (Aeris Technologies, Pico series). The measurement setup, calibration procedures, and a comparison of the setup to mast measurements were described in Vernooij et al. (2022). We calculated EFs using the carbon mass balance method (Ward and Radke, 1993), using ground measurements of the weighted average (WA) carbon content of the combusted fuel and emissions of CO_2, CO, CH_4 and N_2O. The carbon emitted in non-methane hydrocarbons

https://doi.org/10.5194/egusphere-2023-267
Preprint. Discussion started: 6 March 2023

(NMHC) and particulates was estimated based on the linear relations with EFs of CO (for particulates) and CH_4 (for NMHCs), which were derived from previous savanna literature (Andreae, 2019; Vernooij et al., 2022). EFs of N_2O were calculated using CO_2 as the co-emitted carbonaceous reference species.

2.1.2 Sample coverage and literature studies

The dataset obtained using the abovementioned UAS methodology includes both previously published data collected in Mozambique, South Africa, and Brazil (Russell-Smith et al., 2021; Vernooij et al., 2021, 2022) and new measurements from xeric and mesic savannas in Botswana, Zambia and Australia, measured during the fire seasons of 2021 and 2022. The dataset covers three continents and the full length of the dry season, ranging from early dry season (EDS) campaigns in which fuel conditions prevented successful ignition to late dry season (LDS) campaigns with high-intensity fires. The 129 fires that we measured using the abovementioned methodology were supplemented with 85 previous savanna fires for which EFs of the measured species were reported in the updated database by Andreae (2019). This literature compilation only includes samples taken within minutes after emission to avoid significant chemical changes during atmospheric aging. For the comparison with geospatial data, we only included fires for which the fire date and coordinates were known, a prerequisite to get relevant satellite features. These criteria mean that laboratory studies, satellite studies covering wider regions, and most aircraft campaigns were excluded. Fig. 1 provides an overview of the UAS (red for previously published and orange for our new measurements), and literature (yellow) sample locations included in the study.

2.1.3 Fuel measurements

During more recent fieldwork campaigns, we not only collected EFs but also other parameters including fuel characteristics. Before the fire, we collected fuel load and fuel composition from various classes (e.g., grass, litter, coarse woody debris, shrubs and trees) and meteorological parameters. After the fire, we revisited the plots and recorded various fire severity proxies including the combustion completeness of various fuel classes as well as fire intensity proxies (e.g. patchiness of the fire, and scorch and char heights) following the methodology outlined by Eames et al. (2021) and Russell-Smith et al. (2020). Table 1 lists the individual UAS EF-measurement campaigns, and whether fuel was collected following the abovementioned methodology. Fires were lit on the windward side of the plot and generally burned through 2-6 individual randomly scattered 50×10-meter fuel transects covering the target vegetation type and fuel age. We took the average of the affected fuel transects as the fire-averaged value, to correspond to the fire-averaged EF measured over all the bag samples taken from that specific fire.

2.2 Regression analysis

Field measurements provide the most accurate description of the vegetation and weather conditions during the fire and yielded the most reliable insights in the drivers of EF dynamics. However, these measurements are sparse and thus unsuitable for spatiotemporal extrapolation. We therefore build machine learning algorithms, for which we selected a subset of satellite and reanalysis features with global coverage and temporal data availability for at least the past 20 years.

https://doi.org/10.5194/egusphere-2023-267
Preprint. Discussion started: 6 March 2023

2.2.1 Global feature selection

To avoid the model becoming a black box, we did not include features with no intuitive significance or cogent link to EFs (e.g. individual satellite retrieval bands). Table 2 lists the different satellite and reanalysis products included in this study, along with the observed range for each feature over the included fires.

We used remote sensing products based on retrievals from the Moderate Resolution Imaging Spectroradiometer (MODIS) and reanalysis data with sufficient spatial and temporal coverage. Based on the coordinates of the individual samples we obtained a broad range of features which we then averaged over the samples from each individual fire to obtain the fire-averaged feature scores. As proxies for the vegetation conditions and landscape parameters prior to the fire we used Fractional Tree Cover (FTC) and Fractional Bare soil Cover (FBC) from MOD44BC6 (DiMiceli et al., 2015), the Fraction of absorbed Photosynthetically Active Radiation (FPAR) and the Leaf Area Index (LAI), which were retrieved from MCD15A2HC6 (Myneni et al., 2015). Based on MOD09GAC6 surface spectral reflectance (Vermote, 2015), we determined the Normalized Difference Vegetation Index (NDVI) before the fire and the Pgreen (calculated as NDVI before the fire minus the minimum NDVI of the previous year, divided by the total NDVI range of previous year (Korontzi, 2005)).

To estimate the weather conditions during the fire, we used ERA5-land meteorological reanalysis data from the European Centre for Medium Range Weather Forecasts (ECMWF) (Muñoz-Sabater et al., 2021). Hourly meteorological data for air temperature, wind speed, relative humidity, evapotranspiration and potential evapotranspiration were used for the UTC-corrected time stamp of each sample. Based on the timing of the sample, the feature value was obtained using linear temporal interpolation. Temperature and relative humidity were subsequently used to derive the Vapor Pressure Deficit (VPD, i.e. the difference between the saturation vapor pressure and the actual vapor pressure) following the method described by Tetens (1930). The Evaporative Stress Index (ESI) was calculated as the actual evapotranspiration divided by the potential evapotranspiration (Anderson et al., 2007). We used ERA5-land monthly average rainfall data to estimate the mean annual rainfall (MAR) over the 1990–2022 period, as well as the cumulative rainfall in the 12 months prior to the fire. We found meteorological parameters obtained from ERA5-Land (Muñoz-Sabater et al., 2021) to be in close accordance with ERA5 (Hersbach et al., 2020), indicating the two may also be substituted.

Fire weather comprises combinations of weather and fuel parameters that determine the risk of wildfire. Indices like the globally available Fire Weather Index (FWI) have been developed with the aim of estimating the risk of wildfires (De Groot, 1987; Van Wagner, 1987) and are based on global reanalysis data. In this assessment we have included the daily FWI along with some of the intermediate parameters used to calculate the FWI. These intermediate parameters include: (1) the Fine Fuel Moisture Code (FFMC), designed to capture changes in the moisture content of fine fuels and leaf litter, (2) the Drought Code (DC), which captures the moisture content of deep, compacted organic soils and heavy surface fuels, (3) the Build-up Index (BUI) which represents the total fuel availability, and (4) the Initial Spread Index (ISI), which is driven by wind speed and the FFMC, and represents the ability of a fire to spread immediately after ignition. We used the global fire weather indices based on ERA5 (Hersbach et al., 2020) with a 0.25 spatial resolution and 1950-present temporal coverage (Vitolo et al., 2020) that are calculated as part of the European Forest Fire Information System (EFFIS). Global fire weather indices based on ERA5 (Vitolo et al., 2020) had significant inconsistency compared to fire weather indices based

https://doi.org/10.5194/egusphere-2023-267
Preprint. Discussion started: 6 March 2023

on GEOS-5 and MERRA-2 obtained from the Global Fire Weather Database (GFWED; Field et al., 2015), meaning these data should not be used as substitutes. Because of the consistency and higher spatial resolution, we only included ERA5 in our analysis.

For fire severity proxies we used the differential Normalized Burn Ratio (dNBR) and the differential Normalized Difference Vegetation Index (dNDVI) retrieved before and after the fire. These were based on the MODIS surface spectral reflectance, corrected for atmospheric conditions (MOD09GAV6; Vermote, 2015). If the scene before or after the fire was cloud-covered, the preceding or successive scene was used with a limit of 14 days before or after the fire. If no cloud-free scene was available in that time window, the fire was removed from the dataset.

2.2.2 Machine learning methodology

We tested a variety of different regression methodologies for the prediction of the fire-WA EFs based on the abovementioned satellite and reanalysis features. Using the Scikit-learn library in Python (Pedregosa et al., 2011), we trained multiple linear regression, decision tree-, random forest-, gradient boosting machine- and neural network regressors to predict the MCE and the EFs of CO, CO_2, CH_4 and N_2O. Many of the meteorological and fuel characteristics follow seasonal patterns and exhibit strong co-variation. While this may be problematic for linear models, it should not negatively impact the decision-tree-based modes and therefore these features were included in the model. We trained the models using the in-situ EF measurements (both ours and those from literature), to reconstruct the measured EF dynamics. We removed measurements with missing values for any of the included features. The remaining data was divided into training (70%) and validation data (30%), and the training data was resampled using ten-fold cross validation while allowing sample replacement (i.e., bootstrap method). All regression methods were trained to maximize the explained variance in the data. The hyper parameters were tuned using the scikitlearn "GridsearchCV" algorithm (Pedregosa et al., 2011). Random Forest (RF) regressors gave the best results followed by gradient boosting machine (GBM) regressors. We therefore decided to proceed using RF regressors to predict the MCE and the EFs of CO, CO_2, CH_4 and N_2O.

2.3 Spatial extrapolation for global savanna emission estimates

Depending on the required spatial resolution of the EF product, we re-gridded the feature values by averaging features with overlapping grid cells. Figure 2 provides an example for the estimation of the CO EF at 500-meter resolution for MODIS tile "h20v10" (covering parts of Zambia, Botswana, Angola, Namibia, Zimbabwe, Mozambique and the Democratic Republic of the Congo) on June 1st, 2019, using the features shown in Fig 2a-e. The temporal resolution of the EFs in the example of Fig. 2 is daily, in which the day-to-day EF dynamics are being driven by daily variations in VPD, FPAR, FWI and soil moisture. Most burned area products do not differentiate the time of the day at which a grid cell was burned. For features with a typically diurnal pattern, we therefore weighed the hourly meteorological data by the average diurnal fire profile in the respective month for the grid cell. For monthly resolution EFs we did the same using the ERA5-land monthly data averaged by hour of day. This diurnal fire profile was based on the three-hourly fractions of daily emissions obtained from GFED4.1s, which is based on the timing of active fire detections from both MODIS and geostationary satellites (Mu et al., 2011; van der Werf et al., 2017). To study the effect of EF patterns in savannas, we calculated monthly global savanna emissions by multiplying the dynamic EFs with dry matter emissions from GFED4s (Randerson et al., 2012; van der Werf et al., 2017) at 0.25° spatial resolution, for the 2002-2016 period (the period for which MCD64AC5 as used in GFED4s was available). To classify the landcover type of the cell (Fig. 2f) we used the International Geosphere-Biosphere Program (IGBP) classification (Loveland and Belward, 1997), obtained from the MODIS annual MCD12Q1C6 product (Friedl and Sulla-Menashe, 2019), where the savanna biome comprised land cover types classes 6-11 . We then calculated the dynamic monthly EFs at 0.25° spatial resolution for the savanna biome using the RF models for the MCE and the EFs for CO, CH_4, N_2O and CO_2. For burned grid cells that were partially classified as savanna, the EF of the cell was obtained by averaging the EFs of the different biomes in the underlying 500-meter grid cells, weighted by their dry matter emissions. We ran GFED4s using both static (original) and dynamic (this study) EFs for the savanna biome to determine the impact on seasonal and spatial emission patterns using our approach.

3 Results

3.1 Variability of savanna EF measurements

During six fire seasons we have collected over 4500 bag samples containing emissions from 129 fires, in a variety of savanna ecosystems under different seasonal conditions. Figure 3 shows the range, averages (green diamond), and WA EFs (red crosses) measured during the campaigns listed in Table 1. For the calculation of the WA N_2O EF we excluded samples which contained less than 10 moles of total carbon emissions following the findings described by Vernooij et al. (2021). Table A1 provides a short geomorphological and floristic description of the measured savanna ecosystems, including the seasonal behaviour of the dominant vegetation. The relatively small range in the boxplot describing previous savanna literature (Fig. 3, red box) may be attributed to the fact that most studies report either fire-averages, vegetation type averages or even study averages, whereas the other boxplots based on our measurements show the variability observed between individual samples.

We observed substantial variability within different savanna ecosystems which was strongly linked to tree-cover density and mean annual rainfall. EFs of CO and CH_4 were lower in xeric open savannas compared to woodland savannas. Fire-WA EF measurements for CO, CH_4 and N_2O, using the UAS method were on average 13%, 29% and 44% lower than estimates listed in previous inventories. However, this may be largely attributable to the fact that xeric savannas were overly represented in our measurements in terms of annual burned area (i.e. sample bias). Our measurements in higher rainfall savannas were much closer to the previous averages (Fig. 3). In humid areas (e.g. seasonally inundated grasslands), we found large intra-seasonal differences in N_2O, CO and CH_4 EFs. Water availability in these landscape features is often strongly soil type and geomorphology related (Bullock, 1992; Gonçalves et al., 2022), making the correlation with seasonal rainfall less direct and drying patterns over the dry-season more diverse. The grasslands with the highest EFs (found in high-rainfall savanna Dambos) were uncharacteristically green for the time of the season, and fires in these landscapes would therefore not be representative of more xeric grasslands.

https://doi.org/10.5194/egusphere-2023-267
Preprint. Discussion started: 6 March 2023

3.2 EF seasonality, fire intensity dynamics and fuel consumption in xeric and mesic savannas

Table 3 lists the EDS and LDS pre- and post-fire fuel characteristics, averaged over all the transects we measured in the respective vegetation type and season. For some characteristics (e.g. the total fuel load), it is important to note that the columns do not necessarily represent corresponding mixtures of fuel age. For some field campaigns, no nutrient content data was collected from the leaves and stems of shrubs. In both xeric- and mesic savannas, the moisture content of the fuel and the relative humidity were substantially lower in the LDS compared to the EDS. This resulted in increases in fire intensity proxies over the dry season. Particularly during measurement campaigns in the Miombo woodlands in Mozambique and Zambia, the fine fuel in the EDS plots predominantly consisted of tree litter and became even more litter-dominated with the progression of the dry season. EDS fires were patchy, and generally did not consume coarse woody debris and shrubs. As the dry season progressed, there was a clear shift towards the combustion of more Residual Smouldering Combustion (RSC)-prone fuels like coarse woody debris, stems, live foliage, and densely packed litter, which coincided with higher EFs for CO and CH_4 in the LDS. This shift also results in a seasonal increase in the WA carbon content of the consumed fuel of woody savannas (Table 3) which linearly scales the EFs of all measured species.

Overall, our measurements of CO and CH_4 EFs in xeric, grass- and shrub dominated savannas (e.g., Australian spinifex grasslands and open savannas in the Kalahari) were slightly lower in the LDS compared to the EDS campaigns but much lower compared to woody savannas (Fig. 3). Contrary to the woody-dominated savannas, where RSC-prone fuel is readily available and becomes more flammable with the progression of the fire season, fires in xeric shrub and grasslands tended to consume much of the available fuel in the EDS (Table 3). Overall, the WA nitrogen content of the combusted fuel decreased with the progression of the dry season through curing of grasses and litter decomposition. This was somewhat compensated for by an influx of leaf litter and an increased combustion of live shrubs, which were richer in nitrogen than grasses (that had commodiously already cured in the EDS). Overall, fires that consumed more litter emitted more N_2O than grass-dominated fires. Between individual fires, the curing stage of the grasses affected the N_2O EF, with green seasonally-inundated grasslands emitting more N_2O compared to fully cured grasslands. In some miombo woodland fires in Kafue, which were measured in November when the vegetation already carried its first green flush, we also measured relatively high N_2O EFs.

3.3 Estimation of BB EFs using random forest regression based on global features

To extrapolate these relations for use in global models we correlated the field measurements to satellite products. Table 4 lists the correlations of the individual field parameters to the EF measurements, as well as global satellite proxies. The strongest predictors for the MCE and the CO and CH_4 EF were the tree density in the plots, the grass to litter ratio, the combustion completeness and the WA moisture content of the consumed fuel (Table 4). In turn, these parameters were best correlated to the remotely sensed FTC, FBC, VPD and the FWI. EFs for CO and CH_4 are primarily proportionate to the inverse combustion efficiency (i.e. the not fully oxidized compounds) which had a standard deviation of 90% relative to the mean. CO_2, on the other hand is proportionate to the fully combusted carbon fraction which is much larger and more stable with a relative standard deviation of 4.5% compared to its mean. Therefore, the carbon content of the fuel –with a standard deviation of roughly 5%– becomes a dominant factor explaining the variability in CO_2 EFs. The features that strongest correlated with the

https://doi.org/10.5194/egusphere-2023-267
Preprint. Discussion started: 6 March 2023

N_2O EF were the nitrogen to carbon ratio in the combusted fuel and the percentage of grass in the fine fuel (consisting of grass, litter and course woody debris), which in turn correlated with the FBC and the VPD.

For the global estimation of MCE and GHG EFs, we found that RF models performed well with respective out of sample correlation coefficients ranging between 0.80 and 0.99. In Figures 4 and 5, feature importance represents the mean accumulation of the impurity decrease within each tree and is an indication of how much each feature is used as a split to explain the variability in the data. The average MCE in the measurements was slightly higher compared to earlier assessments which were used by GFED4s (red line in Figure 4), which may again be attributable to the dominance of relatively dry savannas. Overall, we found that using only globally available data covering a large (>20 year) timespan, we could recalculate the MCE well with a mean absolute error (MAE) of 0.007, which meant a reduction of the MAE of 62% compared to the static biome-averaged MCE.

Although the features listed in Fig. 4 all have sufficient spatiotemporal coverage for global emission modelling, some features exhibited strong co-variation. Other retrievals were hampered by LDS cloud-cover (e.g., dNBR and Pgreen), which meant we could not use consistent quality retrievals or had to remove samples from the data. Further simplification by excluding these features somewhat remedied these issues and could therefore improve the global applicability, fortunately without losing much explained variance. When using a 5-feature subset, we found that RF regressors still predicted much of the variability in the MCE and EFs. Figure 5a shows the predictive performance of a RF regression model that uses VPD, FTC, FWI, FPAR and soil moisture (SM) to estimate the MCE, which was relatively similar to the model predicting MCE using all features (r of 0.80 vs. 0.86).

We found that spatial variability dominated the total variability in the MCE within the savanna biome with higher combustion efficiency in more xeric and open savannas. To isolate the effect of combustion efficiency in the prediction of individual species and make the model more transparent, we added the computed MCE to the predictor features. Both models that were trained using the full set of features in Table 1 and the 5-feature models identified the computed MCE as one of the primary features explaining of the variability in other EFs. The largest deviation from static EFs (vertical red line in Fig. 5d) was predicted for N_2O. This is partially due to the large number of new fires measured using the UAS system (130 fires versus 6 included literature fires) which on average were 44% lower than the static reference used in GFED4s. The modelled MCE was the main predictor of the N_2O EF, followed by the soil moisture in the top layer (0 - 7cm depth). Somewhat surprisingly, we found soil moisture to correlate more strongly with the tree density in the plot rather than the fuel moisture content (Table 4).

3.4 Impact on global emission estimates using variable savanna emission factors

Both our measurements and the averages in savanna literature compilations (e.g. Akagi et al., 2011; Andreae, 2019) for the savanna biome are subjected to sampling bias, with respect to global savannas. Rather than comparing the average of our savanna measurements to the literature averages, we computed the dynamic EFs using the RF model and subsequently calculated the emissions for the entire savanna biome, which is more indicative of the "effective" EFs and compared this to emissions based on static EFs. Figure 6 shows the relative impact of using variable EFs on annual global savanna fire emissions of CO (a), CH_4 (b) and N_2O (c), averaged over the 2002-2016 period based on GFED4s. The map only shows cells for which the partial coverage of

https://doi.org/10.5194/egusphere-2023-267
Preprint. Discussion started: 6 March 2023

savannas exceeds 50%. In grid cells that are partially (50-99%) covered by savanna, the total impact on emissions is to some degree diluted as the EFs of the non-savanna biomes remained constant.

For CO and CH_4, the dominant effect is a spatial redistribution with higher CO and CH_4 EFs in mesic, high-tree-cover savannas and lower EFs in xeric savannas compared to previous estimates. For CO_2 (not shown), we find the opposite pattern to CO. Relatively speaking, however, changes in CO_2 emission are much smaller because most carbon is emitted as CO_2, even when MCE values are low. Although CO and CH_4 followed the same spatial pattern, we found that MCE affected the CH_4 EF more strongly than the CO EF which resulted in lower CH_4 to MCE ratios in open savannas. Global savanna emissions of CO were 2% higher compared to the GFED4s reference scenario whereas N_2O and CH_4 emissions were respectively 18% and 5% lower. N_2O emissions were lower for the entire savanna biome (Fig. 6c). Over the 2002-2016 period, the annual effective EFs (i.e. weighted by the burned fuel) remained more or less stable over the savanna biome.

Figure 7 shows the seasonal patterns in the average CO EF for different savanna vegetation classes in southern hemisphere Africa. The IGBP savanna subclasses are only used here to indicate the average patterns and are not involved in the EF calculation. We found a stronger and more persistent seasonal decline of the CO EF in xeric grass- and shrublands compared to typical and woody savannas. N_2O EFs showed a similar pattern characterised by a decline over the dry season in the more xeric grass and shrubland savannas while EFs in woody savannas are more stable. The model indicates a reversal of the seasonal trend in typical and woody savannas around August-September, long before these rains start. The coloured areas represent the timing of our field campaigns in this region. Although LDS campaigns were conducted before the first seasonal rains, the graph indicates they may not be indicative of peak-season fires. Figure 8 shows an overview of the relative changes in emissions for the various savanna rich GFED regions. Many of these regions contain both xeric and mesic savannas with contrasting spatial patterns, meaning local differences may be much larger (Fig. 6).

4 Discussion

4.1 Comparison with previous studies

The largest difference compared to previous savanna burning emission estimates is the reduction in N_2O emissions. Rather than being the effect of spatiotemporal dynamics, this reduction resulted from a relatively large number of new N_2O EF measurements that were significantly lower than averages reported by EF compilations. These were 0.21 g kg^{-1} in Andreae and Merlet (2001), 0.20 g kg^{-1} in Akagi et al. (2011), and 0.17 g kg^{-1} in Andreae (2019) while our average value for the field measurements was 0.11 g kg^{-1}. However, in our measurements, xeric savannas are overrepresented. When using the global RF model to extrapolate the measurements over the entire savanna biome the "effective" average N_2O EF –for savanna grid cells at the time of their burning– was 0.16 g kg^{-1}, which is similar to those listed in Andreae (2019). It is known that older studies might overestimate N_2O, due to N_2O formation in stainless steel sample containers (Muzio and Kramlich, 1988). Particularly compared to more recent studies, our EFs were in line with other savanna measurements from South America (0.05-0.07 g kg^{-1}; Hao et al., 1991; Susott et al., 1996), Australia (0.07 – 0.12 g kg^{-1}; Hurst et al., 1994; Meyer et al., 2012; Surawski et al., 2015) and Africa (0.16 g kg^{-1}; Cofer et al., 1996). In accordance with Winter et al. (1999b), we found N_2O EFs to be closely correlated with the nitrogen content of the fuel. Through this relation, we can explain

https://doi.org/10.5194/egusphere-2023-267
Preprint. Discussion started: 6 March 2023

both the spatial distribution observed in Fig. 6c and the different seasonal trends. In line with Susott et al. (1996) and Ward et al. (1992) we found that woody vegetation has higher nitrogen content (Table 3), causing higher N_2O emissions from tree dominated areas. The seasonal reduction in the nitrogen content of the fuel as the vegetation cures (Table 3) coincides with a reduction of the N_2O EF over the dry season (Yokelson et al., 2011; Vernooij et al., 2021). This tends to happen quicker in xeric grass- and shrublands compared to mesic tree-covered areas. On the other hand, as fires get more intense over the dry season, they consume increasingly more litter, coarse fuels and live foliage, provided these fuels are available (Table 3). This increases the WA carbon- and nitrogen contents of the fuel. We found relatively low nitrogen content for Australian open woodland savannas, which was in line with previous studies (Bustamante et al., 2006).

For carbonaceous species our model predicts a spatial redistribution, characterized by higher combustion efficiency in lower tree-cover savannas and lower combustion efficiencies in more woody savannas. Previous research by van Leeuwen and van der Werf (2011) identified multi-linear correlations between EFs of CO_2, CO and CH_4 and environmental drivers resulting in coefficients of determination (r^2) ranging from 0.48 to 0.62. In accordance with their study, we found the FTC to be a strong predictor of the MCE and the CO- and CH_4 EFs (Fig. 9). When denoted in grams per kilogram of dry biomass consumed, EFs of carbonaceous species are dependent on both the combustion efficiency and the carbon content of the fuel. The carbon content is often fixed in global studies (e.g. 45% in Andreae (2019) and Andreae and Merlet (2001) or 50% in Akagi et al. (2011)), with the latter forming the basis of the EFs used in GFED4s that represent the static EF references in this study. However, both the combustion efficiency and the carbon content have a spatial component with higher carbon contents in shrubs and trees compared to grasses (Table 3). For the studied fires, the WA carbon content of the fuel ranged from 40.3 to 49.3%, which linearly scales to a 22% difference in EFs between those extremes. In line with Andreae (2019), we assigned a carbon content of 45% to literature studies for which the carbon content was not reported which was close to our average measured value of 45.8 ± 2.3%. Contrary to previous research which indicated that dryer conditions in the LDS would lead to higher-MCE fires in high-tree-cover savannas (Hoffa et al., 1999; Korontzi et al., 2003a), we found lower MCE in these regions under late-LDS conditions (Fig. 3). In part, this may be because our measurement campaigns missed the peak-season fires when the fires may be hotter (N'Dri et al., 2018). Another explanation is that although the LDS fires were more intense, they consumed much more RSC-prone fuels (Table 3), which may explain the higher CH_4 and CO EFs. Eck et al. (2013) studied seasonal changes of BB particles during 15 annual fire seasons in xeric and mesic savannas in southern Africa using the Aerosol Robotic Network (AERONET). They found a linear trend of the single scattering albedo (SSA), increasing throughout the dry season, which would support a late dry season decrease in MCE. In open savannas, we did observe a slight seasonal decline in CO and CH_4 EFs. We found that LDS fires did not significantly change the composition of the fuel and in these areas, as most of the available fuel was consumed in both the EDS and LDS fires.

In accordance with previous studies (e.g. Korontzi et al., 2003b; van Leeuwen and van der Werf, 2011), we found steeper CH_4 EF to MCE regression slopes in woodlands compared to grasslands. Our data indicated a positive correlation of the CH_4 EF to MCE slope with the FTC from MOD44Bv6. Keep in mind that the MCE is only calculated through CO and CO_2 emissions. Being less oxidized, CH_4 emissions have a stronger dependency on

https://doi.org/10.5194/egusphere-2023-267
Preprint. Discussion started: 6 March 2023

the actual combustion efficiency than CO (which is still common in flaming combustion), and therefore the MCE. Stable carbon isotopes also point to CH_4 emissions being more depleted in heavy carbon (^{13}C) compared to CO, indicating a stronger dominance of RSC in its total emissions (Vernooij et al. 2022b).

While most studies describe the relationship between the CH4 EF and the MCE as being linear (Korontzi et al., 2003b; van Leeuwen and van der Werf, 2011; Selimovic et al., 2018; Yokelson et al., 2003), we found it may be better described using a nonlinear function (Fig. 9), in line with findings by Meyer et al. (2012) for Australian savanna measurements. This may explain why studies that are skewed towards either smouldering- or flaming phase emissions find different CH_4 EF to MCE slopes using linear regressions.

Although higher MAR generally coincides with high FTC, this was not the case for our measurements from Brazil. The measured areas in the EESGT received relatively high MAR (1250–1600 mm yr^{-1}) compared to 850–1250 mm yr^{-1} for Zambian and 890–1100 mm yr^{-1} for Mozambican Miombo woodlands. Nonetheless, although being strictly protected from logging and other land clearing practices, the MOD44BC6 FTC in the measured areas in EESGT was very low (1-10%, with an average of 2%) compared to 7-32% with an average of 19% for Zambian-, and 3-43% with an average of 22% for Mozambican miombo woodlands. That our measurements in the EESGT were skewed towards open savannas (that typically burn with higher MCE), may explain the relatively low CH_4 EF to MCE slope discussed in Vernooij et al. (2021). For the whole Cerrado, the average MOD44BC6 FTC is 17%, indicating that the measurements in EESGT may be underestimating the MCE in other parts of the Cerrado. According to its classification, MCD44Bv6 FTC only includes canopies of trees exceeding 5m in height (Adzhar et al., 2021) which may be why some common Cerrado species are classified as shrubs. However, the EFs observed from these areas were similar to those observed in low tree-cover savannas.

4.2 Model representativeness

This is the first study to quantify the spatial distribution of GHG EFs over the entire savanna biome using field measurements from a variety of savanna ecosystems, based on dynamic satellite data. Although spatiotemporal coverage has improved, there are still many understudied savanna and grassland areas for which we have derived EFs based on our model. Figure 1 clearly illustrates the gaps in the spatial distribution of the training data. Particularly savannas bordering the tropical rainforest, northern hemisphere Africa, meso America, south-east Asia as well as temperate grassland systems are understudied. The absence of measurements in these ecosystems means EFs are currently calculated using measurements from predominantly southern hemisphere Africa. However, Fig. 8 suggests EF dynamics may significantly deviate from those in the well-studied savannas. In order to ensure the representativeness of the model to specific areas, calibration and model evaluation using additional in-situ EF measurements remains necessary.

4.3 Spatial resolution and small-scale landscape features

We found the highest variability of EFs within smaller landscape features that are bound to geomorphological niches, typically along rivers and valleys. While these features are likely to have low significance for global emission patterns, they represent vital ecosystems that may require special fire protection. High-resolution modelling allows for a better understanding of localized fire regimes, especially in relatively heterogeneous

https://doi.org/10.5194/egusphere-2023-267
Preprint. Discussion started: 6 March 2023

landcover regions. In this study we averaged the features over the 0.25° grid cell prior to determining the savanna EF. This approach was chosen because GFED4s burned area, which includes an assumption for small fires, is produced at 0.25° resolution. Recent studies have shown that higher resolution modelling can lead to different emissions partly because landscape heterogeneity is better represented (van Wees and van der Werf, 2019). Next generation global emission models are therefore likely to incorporate increased spatial resolution. Particularly from a land management perspective, having more representative local data is beneficial.

The model is limited by the accuracy and spatial resolution of the underlying products. Using the features included in the current models, EFs can be calculated up to the native resolution of the included MODIS-based products (500×500m), which is also the resolution of globally available burned area products. New high-resolution burned area products, however, indicate that these global products grossly underestimate burned area due to omission of small fires (Roteta et al., 2021; Roy et al., 2019). As this model is trained using specific datasets, these features should not be replaced by other sources without evaluating the consistency of that source to the training datasets. Particularly if the error in the underlying features in inconsistent, this propagates to the EF estimations. FTC and FBC, based on MOD44Bv6 were found to be strong predictors of BB EFs. However, intercomparison with Tropical Biomes in Transition (TROBIT) field sites in African, Brazilian and Australian savannas has shown that this product consistently underestimates canopy cover in tropical savannas by between 9 to 15% (Adzhar et al., 2021). Products based on higher-resolution satellite retrievals (e.g. LandSat and Sentinel) have the potential to further enhance the spatial resolution of the EF estimates to include small landscape features and thus become more representative.

Cross-correlation between the features meant that feature importance scores varied over various model runs based on the test-train data split and bootstrap resampling. For example, a decision tree split based on VPD is most likely very similar to soil moisture or RH, and FTC in national parks is often closely correlated to the MAR, with our measurement sites in Brazil being the notable exception. Although we conducted model runs for various feature-subsets and selected the best, different features may also perform well in explaining much of the variability. For features with very high co-variation (e.g., FPAR and LAI or FWI and ISI), this meant only one feature was selected for the trimmed-down model even when both features scored high on the initial assessment.

5 Conclusion

Over the last decade, substantial progress has been made on increasing the spatiotemporal coverage of savanna fire emission factor measurements (EFs). In this study we described the variability of GHG EFs measured during 18 new field campaigns over the 2017-2022 period during which we measured 129 fires in different parts of the savanna biome using UAS measurements. On average CO, CH_4 and N_2O EFs in these UAS measurements were respectively 13%, 29% and 44% lower compared to the biome-averaged EFs used in previous inventories. However, from a global savanna perspective, xeric savannas with relatively low EFs were over-represented in our measurements which could explain part of the mismatch. Measurements of the pre-and postfire fuel load and the fuel conditions during the fire indicated significant increases in fire intensity over the dry season. Particularly for mesic savannas, an increase in the combustion of RSC-prone fuels resulted in higher EFs of CO and CH_4 during

https://doi.org/10.5194/egusphere-2023-267
Preprint. Discussion started: 6 March 2023

LDS fires. The main drivers of variability in CO and CH_4 EFs were tree-cover, fuel moisture content and the prevalence of grasses while EFs for N_2O strongly correlated with the nitrogen content of the fuel which, in turn, is strongly linked to the grass to litter ratio. Although these correlations are consistent with previous savanna EF studies, quantifying their impact on EFs for the use in global emission studies has so far been hampered by a lack of measurements.

We propose a random forest regressor that estimates dynamic EFs based on satellite retrievals to replace the use of static biome averaged EFs in global emission models, or the use of a dichotomy of EDS vs LDS EFs (based on a cut-off date). The modelled data resulted in significant improvements compared to static biome-averaged EFs, reducing the mean absolute error in the modelled versus measured predictions by 63% for CH_4, 57% for N_2O, 81% for CO and 79% for CO_2. We used the dynamic EF models to calculate the emissions for global savanna emissions over the 2002-2016 period, which is more indicative of the "effective" EF differences. This resulted in a spatial redistribution of emissions over the savanna biome, characterized by increases of average annual emissions of CO, and CH_4 in woody savannas and reductions in open savannas. While the model indicates an initial seasonal decrease in combustion efficiency as the vegetation dried out, there was a reversal for typical and woody savannas towards the end of the dry season, occurring before the first seasonal rains. This shift coincides with the increased consumption of RSC-prone fuels like densely packed litter, coarse woody debris and live vegetation. Xeric savannas had much lower EFs with a longer and more profound seasonal decrease in CO and CH_4. Although N_2O EFs were lower for the entire savanna biome, they followed a similar spatiotemporal pattern.

The proposed dynamic EF method resulted in a 18% reduction in the estimated annual global N_2O emissions from savanna fires, compared to static averages, with emission reductions of up to 60% in xeric regions. The impact on the global savanna emission estimates for CO (increase of 1.8%) and CH_4 (decrease of 2.1%) was low, indicating the use of static EFs did not lead to biases for studies focusing on global emissions. However, the regional impact on these EF estimates was as high as 60% and even 80% under extreme seasonal conditions, highlighting its significance at a more local level. Overall, the model results indicate a first step towards more dynamic and area specific emission models, which will further improve as more measurements and better remote sensing products become available.

Data availability:

The data table containing the training data used for this article along with an explanatory table are available online at: 10.5281/zenodo.7689032 (Vernooij, 2023). Model results are available upon request.

Author contribution:

RV and GRvdW designed the study; RV, TE, JRS, CY, RB, JE, AE, NR, MW, TS, MG, MB, MC and CB conducted the field measurements; RV conducted the analyses on the samples; RV performed the random forest modelling and global analyses and wrote the manuscript with help from DvW and GRvdW.

Competing interests: The authors declare no competing interests

https://doi.org/10.5194/egusphere-2023-267
Preprint. Discussion started: 6 March 2023

Acknowledgements

This research was supported by the Netherlands organization for Scientific Research (NWO) (Vici scheme research programme, no. 016.160.324) and the Ammodo Science Award (2017) for Natural Sciences. The measurement campaigns in Botswana received funding from the International Savanna Fire Management Initiative (ISFMI) and Australia's department of foreign affairs and trade while the field campaigns in Zambia in 2021 and 2022 were partially funded by the United Nations green climate fund. We owe great thanks for the contributions of countless individuals and institutions that provided the permissions, oversight, logistics and expertise needed to perform the field measurements in a safe and coordinated fashion. Among others this has been made possible thanks to 321 Fire, the Brazilian Instituto Chico Mendes de Conservação da Biodiversidade, South African National Parks, the Botswana department of forestry and range resources, the Tsodilo community development trust, the Zambian department of forestry, the wildlife conservation society, the administração nacional das Áreas de Conservação in Mozambique, the Australian central land council and the Yanunijarra aboriginal corporation.

https://doi.org/10.5194/egusphere-2023-267
Preprint. Discussion started: 6 March 2023

Literature

Adzhar, R., Kelley, D., Dong, N., Torello Raventos, M., Veenendaal, E., Feldpausch, T., Philips, O., Lewis, S., Sonké, B., Taedoumg, H., Schwantes Marimon, B., Domingues, T., Arroyo, L., Djagbletey, G., Saiz, G. and Gerard, F.: Assessing MODIS Vegetation Continuous Fields tree cover product (collection 6): performance and applicability in tropical forests and savannas, Biogeosciences Discuss., (February), 1–20, 2021.

Akagi, S. K., Yokelson, R. J., Wiedinmyer, C., Alvarado, M. J., Reid, J. S., Karl, T., Crounse, J. D. and Wennberg, P. O.: Emission factors for open and domestic biomass burning for use in atmospheric models, Atmos. Chem. Phys., 11(9), 4039–4072, doi:10.5194/acp-11-4039-2011, 2011.

Anderson, M. C., Norman, J. M., Mecikalski, J. R., Otkin, J. A. and Kustas, W. P.: A climatological study of evapotranspiration and moisture stress across the continental United States based on thermal remote sensing: 1. Model formulation, J. Geophys. Res. Atmos., 112(10), 1–17, doi:10.1029/2006JD007506, 2007.

Andreae, M. O.: Emission of trace gases and aerosols from biomass burning – an updated assessment, Atmos. Chem. Phys., 8523–8546, 2019.

Andreae, M. O. and Merlet, P.: Emission of trace gases and aerosols from biomass burning, Biogeochemistry, 15(4), 955–966, doi:10.1029/2000GB001382, 2001.

Bullock, A.: Dambo hydrology in southern Africa-review and reassessment, J. Hydrol., 134(1–4), 373–396, doi:10.1016/0022-1694(92)90043-U, 1992.

Bustamante, M. M. C., Medina, E., Asner, G. P., Nardoto, G. B. and Garcia-Montiel, D. C.: Nitrogen cycling in tropical and temperate savannas, Biogeochemistry, 79(1–2), 209–237, doi:10.1007/s10533-006-9006-x, 2006.

Chen, L. W. A., Verburg, P., Shackelford, A., Zhu, D., Susfalk, R., Chow, J. C. and Watson, J. G.: Moisture effects on carbon and nitrogen emission from burning of wildland biomass, Atmos. Chem. Phys., 10(14), 6617–6625, doi:10.5194/acp-10-6617-2010, 2010.

Cofer, W. R., Levine, J. S., Winstead, E. L., Cahoon, D. R., Sebacher, D. I., Pinto, P. and Stocks, B. J.: Source compositions of trace gases released during African savanna fires, J. Geophys. Res., 101, 23,597-23,602, 1996.

DiMiceli, C., Carroll, M., Sohlberg, R., Kim, D., Kelly, M. and Townshend, J.: MOD44B MODIS/Terra Vegetation Continuous Fields Yearly L3 Global 250m SIN Grid V006 [Data set], NASA EOSDIS L. Process. DAAC, doi:10.5067/MODIS/MOD44B.006, 2015.

Eck, T. F., Holben, B. N., Reid, J. S., Mukelabai, M. M., Piketh, S. J., Torres, O., Jethva, H. T., Hyer, E. J., Ward, D. E., Dubovik, O., Sinyuk, A., Schafer, J. S., Giles, D. M., Sorokin, M., Smirnov, A. and Slutsker, I.: A seasonal trend of single scattering albedo in southern African biomass-burning particles : Implications for satellite products and estimates of emissions for the world ' s largest biomass-burning source, J. Geophys. Res. Atmos., 118, 6414–6432, doi:10.1002/jgrd.50500, 2013.

Field, R. D., Spessa, A. C., Aziz, N. A., Camia, A., Cantin, A., Carr, R., De Groot, W. J., Dowdy, A. J., Flannigan, M. D., Manomaiphiboon, K., Pappenberger, F., Tanpipat, V. and Wang, X.: Development of a Global Fire Weather Database, Nat. Hazards Earth Syst. Sci., 15(6), 1407–1423, doi:10.5194/nhess-15-1407-2015, 2015.

Friedl, M. and Sulla-Menashe, D.: MCD12Q1 MODIS/Terra+Aqua Land Cover Type Yearly L3 Global 500m SIN Grid V006 [Data set]., NASA EOSDIS L. Process. DAAC, doi:10.5067/MODIS/MCD12Q1.006, 2019.

Gonçalves, R. V. S., Cardoso, J. C. F., Oliveira, P. E., Raymundo, D. and de Oliveira, D. C.: The role of topography, climate, soil and the surrounding matrix in the distribution of Veredas wetlands in central Brazil, Wetl. Ecol. Manag., 30(6), 1261–1279, doi:10.1007/s11273-022-09895-z, 2022.

De Groot, W. J.: Interpreting the canadian forest fire weather index (FWI) system, in Fourth Central Regional Fire Weather Committee Scientific and Technical Seminar, pp. 3–14, Canadian Forestry Service, Northern Forestry Centre, Edmonton, Alberta., 1987.

Hao, W. M., Scharffe, D., Lob, J. M. and Crutzen, P. J.: Emissions of N20 from the Burning of Biomass in an Experimental System, Geophys. Res. Lett., 18(6), 999–1002, 1991.

Hoffa, E. A., Ward, D. E., Hao, W. M., Susott, R. A. and Wakimoto, R. H.: Seasonality of carbon emissions from biomass burning in a Zambian savanna, J. Geophys. Res., 104(D11), 13841–13853, doi:10.1029/1999JD900091, 1999.

Hurst, D. F., Griffith, D. W. T., Carras, J. N., Williams, D. j. and Fraser, P. J.: Measurements of trace gases emitted by Australian savanna fires during the 1990 dry season, J. Atmos. Chem., 18(1), 33–56, doi:10.1007/BF00694373, 1994.

Kaiser, J. W., Heil, A., Andreae, M. O., Benedetti, A., Chubarova, N., Jones, L., Morcrette, J. J., Razinger, M., Schultz, M. G., Suttie, M. and Van Der Werf, G. R.: Biomass burning emissions estimated with a global fire assimilation system based on observed fire radiative power, Biogeosciences, doi:10.5194/bg-9-527-2012, 2012.

Korontzi, S.: Seasonal patterns in biomass burning emissions from southern African vegetation fires for the year 2000, Glob. Chang. Biol., 11(10), 1680–1700, doi:10.1111/j.1365-2486.2005.001024.x, 2005.

Korontzi, S., Justice, C. O. and Scholes, R. J.: Influence of timing and spatial extent of savanna fires in southern Africa on atmospheric emissions, J. Arid Environ., 395–404, doi:10.1006/jare.2002.1098, 2003a.

Korontzi, S., Ward, D. E., Susott, R. A., Yokelson, R. J., Justice, C. O., Hobbs, P. V., Smithwick, E. A. H. and Hao, W. M.: Seasonal variation and ecosystem dependence of emission factors for selected trace gases and PM 2.5 for southern African savanna fires, J. Geophys. Res. Atmos., 108(D24), doi:10.1029/2003JD003730, 2003b.

van Leeuwen, T. T. and van der Werf, G. R.: Spatial and temporal variability in the ratio of trace gases emitted from biomass burning, Atmos. Chem. Phys., 11(8), 3611–3629, doi:10.5194/acp-11-3611-2011, 2011.

Loveland, T. R. and Belward, A. S.: The International Geosphere Biosphere Programme Data and Information System global land cover data set (DISCover), Acta Astronaut., 41(4–10), 681–689, doi:10.1016/S0094-5765(98)00050-2, 1997.

Meyer, C. P., Cook, G. D., Reisen, F., Smith, T. E. L., Tattaris, M., Russell-Smith, J., Maier, S. W., Yates, C. P. and Wooster, M. J.: Direct measurements of the seasonality of emission factors from savanna fires in northern Australia, J. Geophys. Res. Atmos., 117(D20), doi:10.1029/2012JD017671, 2012.

Mu, M., Randerson, J. T., Van Der Werf, G. R., Giglio, L., Kasibhatla, P., Morton, D., Collatz, G. J., Defries, R. S., Hyer, E. J., Prins, E. M., Griffith, D. W. T., Wunch, D., Toon, G. C., Sherlock, V. and Wennberg, P. O.: Daily and 3-hourly variability in global fire emissions and consequences for atmospheric model predictions of carbon monoxide, J. Geophys. Res. Atmos., 116(24), 1–19, doi:10.1029/2011JD016245, 2011.

Muñoz-Sabater, J., Dutra, E., Agustí-Panareda, A., Albergel, C., Arduini, G., Balsamo, G., Boussetta, S., Choulga, M., Harrigan, S., Hersbach, H., Martens, B., Miralles, D. G., Piles, M., Rodríguez-Fernández, N. J., Zsoter, E., Buontempo, C. and Thépaut, J. N.: ERA5-Land: A state-of-the-art global reanalysis dataset for land applications, Earth Syst. Sci. Data, 13(9), 4349–4383, doi:10.5194/essd-13-4349-2021, 2021.

Muzio, L. J. and Kramlich, J. C.: An artifact in the measurement of N2O from combustion sources, Geophys. Res. Lett., 15, 1369–1372, doi:https://doi.org/10.1029/GL015i012p01369, 1988.

Myneni, R., Knyazikhin, Y. and Park, T.: MCD15A2H MODIS/Terra+Aqua Leaf Area Index/FPAR 8-day L4 Global 500m SIN Grid V006 [Data set], , doi:10.5067/MODIS/MCD15A2H.006, 2015.

N'Dri, A. B., Soro, T. D., Gignoux, J., Dosso, K., Koné, M., N'Dri, J. K., Koné, N. A. and Barot, S.: Season affects fire behavior in annually burned humid savanna of West Africa, Fire Ecol., 14(2), 5, doi:10.1186/s42408-018-0005-9, 2018.

Pedregosa, F., Varoquaux, G., Gramfort, A., Michel, V., Thirion, B., Grisel, O., Blondel, M., Prettenhofer, P., Weiss, R., Dubourg, V. and Vanderplas, J.: Scikit-learn: Machine Learning in Python Fabian, J. Mach. Learn. Res., 12, 2825–2830, 2011.

Randerson, J. T., Chen, Y., Van Der Werf, G. R., Rogers, B. M. and Morton, D. C.: Global burned area and biomass burning emissions from small fires, J. Geophys. Res. Biogeosciences, 117(4), doi:10.1029/2012JG002128, 2012.

Roteta, E., Bastarrika, A., Franquesa, M. and Chuvieco, E.: Landsat and sentinel-2 based burned area mapping tools in google earth engine, Remote Sens., 13(4), 1–30, doi:10.3390/rs13040816, 2021.

Roy, D. P., Huang, H., Boschetti, L., Giglio, L., Yan, L., Zhang, H. H. and Li, Z.: Landsat-8 and Sentinel-2 burned area mapping - A combined sensor multi-temporal change detection approach, Remote Sens. Environ., 231(October 2018), 111254, doi:10.1016/j.rse.2019.111254, 2019.

Russell-smith, J., Yates, C., Vernooij, R., Eames, T., Werf, G. Van Der, Ribeiro, N., Edwards, A., Beatty, R., Lekoko, O., Mafoko, J., Monagle, C. and Johnston, S.: Opportunities and challenges for savanna burning emissions abatement in southern Africa, J. Environ. Manage., 288(March), 112414, doi:10.1016/j.jenvman.2021.112414, 2021.

Russell-Smith, J., Cook, G. D., Cooke, P. M., Edwards, A. C., Lendrum, M., Meyer, C. (Mick) and Whitehead, P. J.: Managing fire regimes in north Australian savannas: applying Aboriginal approaches to contemporary global problems, Front. Ecol. Environ., 11(s1), e55–e63, doi:10.1890/120251, 2013.

Schmidt, I. B., Moura, L. C., Ferreira, M. C., Eloy, L., Sampaio, A. B., Dias, P. A. and Berlinck, C. N.: Fire

https://doi.org/10.5194/egusphere-2023-267
Preprint. Discussion started: 6 March 2023

management in the Brazilian savanna: First steps and the way forward, J. Appl. Ecol., 55(5), 2094–2101, doi:10.1111/1365-2664.13118, 2018.

Selimovic, V., Yokelson, R. J., Warneke, C., Roberts, J. M., De Gouw, J., Reardon, J. and Griffith, D. W. T.: Aerosol optical properties and trace gas emissions by PAX and OP-FTIR for laboratory-simulated western US wildfires during FIREX, Atmos. Chem. Phys., 18(4), 2929–2948, doi:10.5194/acp-18-2929-2018, 2018.

Surawski, N. C., Sullivan, A. L., Meyer, C. P., Roxburgh, S. H. and Polglase, P. J.: Greenhouse gas emissions from laboratory-scale fires in wildland fuels depend on fire spread mode and phase of combustion, Atmos. Chem. Phys., 15(9), 5259–5273, doi:10.5194/acp-15-5259-2015, 2015.

Susott, R. A., Olbu, G., Baker, S. P., Ward, D. E., Kauffman, J. B. and Shea, R. W.: Carbon, hydrogen, nitrogen, and thermogravimetric analysis of tropical ecosystem biomass, in Biomass Burning and Global Change: Remote sensing, modeling and inventory Development and Biomass Burning in Africa, edited by J. S. Levine, pp. 350–360, MIT Press, Cambridge, Mass., 1996.

Tetens, O.: Uber einige meteorologische Begriffe, Zeitschrift fur Geophys., 6, 297–309, 1930.

Urbanski, S.: Forest Ecology and Management Wildland fire emissions , carbon , and climate : Emission factors, For. Ecol. Manage., 317, 51–60, doi:10.1016/j.foreco.2013.05.045, 2014.

Vermote, E.: MOD09A1 MODIS Surface Reflectance 8-Day L3 Global 500m SIN Grid V006, NASA EOSDIS L. Process. DAAC, doi:10.5067/MODIS/MOD09A1.006, 2015.

Vernooij, R.: Measurements of savanna landscap fire emission factors for CO2, CO, CH4 and N2O using a UAV-based sampling methodology, Zenodo [data set], doi:10.5281/zenodo.7689032, 2023.

Vernooij, R., Giongo, M., Assis Borges, M., Costa, M. M., Carolina Sena Barradas, A. and Van Der Werf, G. R.: Intraseasonal variability of greenhouse gas emission factors from biomass burning in the Brazilian Cerrado, Biogeosciences, 18(4), 1375–1393, doi:10.5194/bg-18-1375-2021, 2021.

Vernooij, R., Winiger, P., Wooster, M., Strydom, T., Poulain, L., Dusek, U., Grosvenor, M., Roberts, G. J., Schutgens, N. and Werf, G. R. Van Der: A quadcopter unmanned aerial system (UAS)-based methodology for measuring biomass burning emission factors, Atmos. Meas. Tech., 15(July), 4271–4294, doi:10.5194/amt-15-4271-2022, 2022a.

Vernooij, R., Dusek, U., Popa, M. E., Yao, P., Shaikat, A., Qiu, C., Winiger, P., van der Veen, C., Eames, T. C., Ribeiro, N. and van der Werf, G. R.: Stable carbon isotopic composition of biomass burning emissions – implications for estimating the contribution of C3 and C4 plants, Atmos. Chem. Phys., 22(4), 2871–2890, doi:10.5194/acp-22-2871-2022, 2022b.

Vitolo, C., Di Giuseppe, F., Barnard, C., Coughlan, R., San-Miguel-Ayanz, J., Libertá, G. and Krzeminski, B.: ERA5-based global meteorological wildfire danger maps, Sci. Data, 7(1), 1–11, doi:10.1038/s41597-020-0554-z, 2020.

Van Wagner, C. E.: Development and structure of the Canadian forest fire weather index system. [online] Available from: http://scholar.google.com/scholar?hl=en&btnG=Search&q=intitle:Development+and+Structure+of+the+Canadian+Forest+Fire+Weather+Index+System#0, 1987.

Ward, D. E. and Radke, L. F.: Emissions Measurements from Vegetation Fires : A Comparative Evaluation of Methods and Results, in Fire in the Environment: The Ecological, Atmospheric, and Climatic Importance of Vegetation Fires, edited by P. J. . Crutzen and J. G. Goldammer, pp. 53–76, Chischester, England., 1993.

Ward, D. E., Susott, R. A., Kauffman, J. B., Babbitt, R. E., Cummings, D. L., Dias, B., Holben, B. N., Kaufman, Y. J., Rasmussen, R. A. and Setzer, A. W.: Smoke and fire characteristics for cerrado and deforestation burns in Brazil: BASE-B Experiment, J. Geophys. Res., 97(D13), 14601–14619, doi:10.1029/92JD01218, 1992.

van Wees, D. and van der Werf, G. R.: Modelling African biomass burning emissions and the effect of spatial resolution, Geosci. Model Dev. Discuss., 1–43, doi:10.5194/gmd-2019-116, 2019.

van der Werf, G. R., Randerson, J. T., Giglio, L., Van Leeuwen, T. T., Chen, Y., Rogers, B. M., Mu, M., Van Marle, M. J. E., Morton, D. C., Collatz, G. J., Yokelson, R. J. and Kasibhatla, P. S.: Global fire emissions estimates during 1997-2016, Earth Syst. Sci. Data, 9(2), 697–720, doi:10.5194/essd-9-697-2017, 2017.

Winter, F., Wartha, C. and Hofbauer, H.: The Relative Importance of Radicals on the N2O and NO Formation and Destruction Paths in a Quartz CFBC, J. Energy Resour. Technol., 121(2), 131–136, doi:10.1115/1.2795068, 1999.

Yokelson, R. J., Bertschi, I. T., Christian, T. J., Hobbs, P. V., Ward, D. E. and Hao, W. M.: Trace gas

https://doi.org/10.5194/egusphere-2023-267
Preprint. Discussion started: 6 March 2023

measurements in nascent, aged, and cloud-processed smoke from African savanna fires by airborne Fourier transform infrared spectroscopy (AFTIR), J. Geophys. Res. Atmos., 108(13), doi:10.1029/2002jd002322, 2003.

Yokelson, R. J., Burling, I. R., Urbanski, S. P., Atlas, E., Adachi, K., Buseck, P. R., Wiedinmyer, C., Akagi, S. K., Toohey, D. W. and Wold, C. E.: Trace gas and particle emissions from open biomass burning in Mexico, Atmos. Chem. Phys., 11(14), 6787–6808, doi:10.5194/acp-11-6787-2011, 2011.

https://doi.org/10.5194/egusphere-2023-267
Preprint. Discussion started: 6 March 2023

Tables

Table 1: Measurement campaigns including the number of fires for which emission factors were measured as well as the number of corresponding fuel-transects.

Area	Timeframe	# Fires	# Fuel transects
Kruger National Park, South Africa	29.08.2017 – 02.09.2017	3	-
	22.04.2018 – 28.04.2018	3	-
	21.08.2018 – 31.08.2018	8	-
	22.10.2018 – 26.10.2018	6	-
Estação Ecológica Serra Geral do Tocantins, Brazil	10.09.2017 – 20.09.2017	10	-
	15.06.2018 – 30.06.2018	11	-
	21.09.2018 – 12.10.2018	6	-
North-west Ngamiland, Botswana	21.05.2019 – 08.06.2019	5	39
	04.09.2019 – 15.09.2019	6	37
Niassa special reserve Mozambique	19.06.2019 – 09.07.2019	10	20
	05.10.2019 – 20.10.2019	11	24
Kasane Extension Forest Reserve, Botswana	12.10.2021 – 20.10.2021	2	42
Bovu Forest Reserve, Zambia	22.10.2021 – 26.10.2021	3	9
Kafue national park, Zambia	30.10.2021 – 12.11.2021	6	54
	15.06.2022 – 20.06.2022	5	24
Lualaba Forest Reserve, Zambia	21.06.2022 – 25.06.2022	5	60
Tanami desert, Australia	20.04.2022 – 28.04.2022	10	90
	12.08.2022 – 05.09.2022	6	24

https://doi.org/10.5194/egusphere-2023-267
Preprint. Discussion started: 6 March 2023

Table 2: Satellite reanalysis features assessed for the prediction of savanna biomass burning emission factors

	Parameter	Data source	Product reference	Spatial resolution	Temporal resolution	Feature range
Vegetation parameters	Fraction tree cover (FTC, %)	MODIS	MOD44BC6 (DiMiceli et al., 2015)	500×500 meter	year^{-1}	0 – 53%
	Fraction bare soil cover (FBC, %)	MODIS	MOD44BC6 (DiMiceli et al., 2015)	500×500 meter	year^{-1}	1 – 88%
	Time since the last fire (years)	MODIS	MCD64A1C6 (Giglio et al., 2018)	500×500 meter	year^{-1}	1 – >10 years
	Normalized difference vegetation index (NDVI) before fire	MODIS	MOD09GAC6 (Vermote, 2015)	500×500 meter	day^{-1}	0.02 – 0.79
	Fraction of absorbed photosynthetically active radiation (FPAR)	MODIS	MCD15A2HC6 (Myneni et al., 2015)	500×500 meter	8 days^{-1}	0.09 – 0.75
	Leaf area index (LAI)	MODIS	MCD15A2HC6 (Myneni et al., 2015)	500×500 meter	8 days^{-1}	2 – 30
	Leaf area index (LAI) Low vegetation	Reanalysis	ERA5-Land (Muñoz-Sabater et al., 2021)	0.1×0.1 degree	day^{-1}	0.5 – 2.0
	Leaf area index (LAI) High vegetation	Reanalysis	ERA5-Land (Muñoz-Sabater et al., 2021)	0.1×0.1 degree	day^{-1}	0.0 – 5.0
	Mean annual rainfall (MAR)(mm)	Reanalysis	ERA5-Land (Muñoz-Sabater et al., 2021)	0.1×0.1 degree	month^{-1}	200 – 1550
Seasonal parameters	Rainfall in the last 12 months (mm)	Reanalysis	ERA5 (Hersbach et al., 2020)	0.25×0.25 degree	month^{-1}	220 – 1550
	Rainfall since the last fire (mm)	Reanalysis	ERA5 (Hersbach et al., 2020)	0.25×0.25 degree	month^{-1}	220 – 11300
	Percentage green vegetation (%) (Korontzi, 2005)	MODIS	MOD09GAC6 (Vermote, 2015)	500×500 meter	day^{-1}	2 – 89
	Soil moisture content ($m^3 m^{-3}$) in the top layer (0 - 7cm depth)	Reanalysis	ERA5-Land (Muñoz-Sabater et al., 2021)	0.1×0.1 degree	hour^{-1}	0.01 – 0.43
	Vapor pressure deficit (mbar)	Reanalysis	ERA5-Land (Muñoz-Sabater et al., 2021)	0.1×0.1 degree	hour^{-1}	8 – 51
	Evaporative stress index (index)	Reanalysis	ERA5-Land (Muñoz-Sabater et al., 2021)	0.1×0.1 degree	hour^{-1}	0.02 – 0.73
Weather	Temperature at 2m (°C)	Reanalysis	ERA5-Land (Muñoz-Sabater et al., 2021)	0.1×0.1 degree	hour^{-1}	16 – 36
	Windspeed (m sec^{-1})	Reanalysis	ERA5-Land (Muñoz-Sabater et al., 2021)	0.1×0.1 degree	hour^{-1}	0 – 11.2
	Relative humidity (%)	Reanalysis	ERA5-Land (Muñoz-Sabater et al., 2021)	0.1×0.1 degree	hour^{-1}	8 – 71
	Canadian Fire Weather Index (FWI)	Reanalysis	CEMS EFFIS (Vitolo et al., 2020)	0.25×0.25 degree	day^{-1}	10 – 102
	Fine Fuel Drought Code (FFDC)	Reanalysis	CEMS EFFIS (Vitolo et al., 2020)	0.25×0.25 degree	day^{-1}	81 – 99
	Initial Spread Index (ISI)	Reanalysis	CEMS EFFIS (Vitolo et al., 2020)	0.25×0.25 degree	day^{-1}	1.9 – 47.5
Fire intensity indices	Build up index (BUI)	Reanalysis	CEMS EFFIS (Vitolo et al., 2020)	0.25×0.25 degree	day^{-1}	64 – 624
	Differential normalized difference vegetation index (dNDVI)	MODIS	MOD09GAC6 (Vermote, 2015)	500×500 meter	day^{-1}	-0.43 – 0.61
	Differential normalized burn ratio (dNBR)	MODIS	MOD09GAC6 (Vermote, 2015)	500×500 meter	day^{-1}	-0.25 – 0.45

https://doi.org/10.5194/egusphere-2023-267
Preprint. Discussion started: 6 March 2023

Table 3: Consumption of RSC-prone fuels in the EDS and LDS for xeric open savannas measured in Botswana and Australia and Miombo woodlands measured in Mozambique and Zambia.

Field measurements before and after burning	Xeric savannas (500 - 750 mm year^{-1} MAR)				Mesic savannas (750 - 1500 mm year^{-1} MAR)			
	Australian arid open woodland		Kalahari open woodland		Kafue woodland savanna		Niassa woodland savanna	
	EDS	LDS	EDS	LDS	EDS	LDS	EDS	LDS
Fine fuel load (tonne ha^{-1})	5.1	6.7	3.1	3.4	2.8	5.9	6.3	5.4
Grass percentage of total fine fuel (i.e. grass, litter and coarse)	76%	79%	27%	25%	24%	17%	45%	35%
Nitrogen to Carbon ratio[1]	1.0%	0.8%	2.3%	2.1%	-	1.7%	1.3%	1.1%
WA Carbon content[1]	45.2%	44.6%	49.1%	47.8%	-	46.5%	43.5%	46.2%
Grass	45.1%	43.9%	47.6%	47.5%	-	47.0%	43.0%	44.0%
Litter	45.2%	47.0%	50.1%	48.0%	-	46.7%	43.2%	47.2%
Coarse woody debris	48.1%	48.0%	48.2%	47.7%	-	44.7%	47.2%	47.8%
Shrub stems[2]	-	47.1%	47.9%	-	-	47.5%	-	48.2%
Shrub foliage[2]	-	50.0%	50.3%	-		51.6%	-	50.7%
WA Nitrogen content	0.45%	0.37%	1.11%	1.00%	-	0.81%	0.55%	0.52%
Grass	0.46%	0.31%	1.06%	0.65%	-	0.42%	0.34%	0.30%
Litter	0.43%	0.65%	1.22%	1.17%	-	0.92%	0.73%	0.65%
Coarse woody debris	0.33%	0.48%	0.89%	0.69%	-	0.61%	0.42%	0.48%
Shrub stems[2]	-	0.63%	1.10%	-	-	0.65%	-	0.52%
Shrub foliage[2]	-	1.03%	2.55%	-		2.02%	-	1.13%
Relative humidity (air)	18%	10%	13%	6%	22%	17%	24%	19%
Fuel moisture content[1]	15.6%	8.6%	20.3%	8.7%	16.5%	6.5%	16.6%	8.8%
Fine fuel combusted	93%	97%	69%	75%	58%	77%	60%	71%
Coarse fuel combusted (∅ < 5cm)	21%	17%	21%	16%	4%	26%	2%	19%
Heavy fuels combusted (∅ > 5cm)	76%	32%	3%	35%	0%	16%	2%	8%
0-50 Cm shrubs combusted:								
Leaves[2]	72%	86%	50%	60%	17%	79%	20%	71%
Stems	60%	65%	38%	88%	1%	44%	24%	40%
50-100 Cm shrubs combusted:								
Leaves[2]	51%	78%	26%	48%	7%	43%	46%	55%
Stems[2]	60%	65%	19%	8%	0%	15%	3%	20%
100-200 Cm shrubs combusted:								
Leaves	26%	69%	22%	31%	0%	47%	20%	35%
Stems	7%	13%	4%	3%	0%	5%	4%	11%
>200 Cm shrubs combusted:								
Leaves	33%	36%	10%	16%	0%	10%	7%	43%
Stems	5%	7%	0%	1%	0%	3%	2%	4%
Scorch height (m)	2.0 m	2.2 m	0.4 m	0.4 m	0.3 m	10.3 m	0.5 m	1.7 m
Char height (m)	0.9 m	1.1 m	0.2 m	0.3m	0.2 m	0.9 m	0.4 m	1.6 m
Patchiness (% burned)	69%	94%	51%	72%	54%	99%	63%	95%

[1]weighted average over the consumed contribution of each individual fuel subclass.
[2]weighted average over the dominant shrub types found in the plots.

https://doi.org/10.5194/egusphere-2023-267
Preprint. Discussion started: 6 March 2023

Table 4. Spearman correlation matrix for the field measurements and the globally available satellite products. Positive correlations are presented in blue while negative correlations are presented in red.

	MCE	CH_4 emission factor	CO emission factor	CO_2 emission factor	N_2O emission factor
Temperature (°C) Drone	-0.21	0.28	0.15	-0.37	-0.05
Rel Humidity (%) Drone	-0.32	0.28	0.3	-0.2	0.03
Fuel moisture content (%)	-0.48	0.47	0.37	-0.64	-0.01
Trees per hectacte	-0.49	0.47	0.42	-0.37	-0.13
Average tree height (m)	-0.4	0.39	0.37	-0.16	0.07
% grass of total dry Fine fuel	0.27	-0.32	-0.33	-0.37	-0.46
Total fine fuel (tonne ha^{-1})	-0.04	0.16	-0.03	-0.47	-0.2
Combustion completeness fine fuel (%)	0.58	-0.5	-0.6	-0.02	-0.35
Combustion completeness coarse fuel (%)	0.17	-0.08	-0.14	0.38	0.06
Combustion completeness heavy fuel (%)	0.19	-0.2	-0.2	0.06	0.13
Char height (cm)	0.34	-0.19	-0.38	-0.15	-0.26
Scorch height (cm)	0.41	-0.13	-0.42	0.06	-0.19
Patchiness (Surface percentage burned)	0.01	0.11	-0.09	-0.49	0.06
Nitrogent to Carbon (ratio)	-0.16	0.18	0.25	0.61	0.56
nitrogen content grass	0.22	-0.2	-0.15	0.55	0.23
carbon content grass	0.1	-0.06	0.02	0.77	0.4
nitrogen litter grass	-0.15	0.18	0.24	0.51	0.59
carbon content litter	0.09	-0.13	0.03	0.58	0.31
average Carbon content	-0.08	0.09	0.21	0.75	0.38
average Nitrogen content	-0.18	0.2	0.27	0.57	0.55

	Years since last burn (MODIS)	Fraction bare soil (%) (MODIS)	Fraction tree cover (%) (MODIS)	Vapor pressure deficit (mbar) (ERA5-land)	Relative humidity (%) (ERA5-land)	Evaporative stress index (ratio) (ERA5-land)	windspeed (m/s) (ERA5-land)	Temperature (°C) (ERA5-land)	Soil moisture (m^3 m^{-3}) (ERA5-land)	mean annual rainfall (mm) (ERA5-land)	last years rainfall (mm) (ERA5)	rainfall since last fire (mm) (ERA5)
Temperature (°C) Drone	-0.24	-0.07	0.16	0.23	-0.12	-0.13	-0.1	0.18	-0.11	-0.23	-0.15	-0.3
Rel Humidity (%) Drone	-0.12	-0.46	0.41	-0.07	0.34	0.45	-0.15	0.13	0.4	0.37	0.32	0.1
Fuel moisture content (%)	0.09	0.32	-0.24	-0.35	0.18	-0.3	0.02	-0.2	-0.21	-0.09	-0.26	0.1
Trees per hectacte	-0.24	-0.75	0.64	-0.05	0.33	0.75	-0.19	0.11	0.57	0.55	0.6	0.09
Average tree height (m)	-0.13	-0.63	0.51	0.13	0.19	0.62	-0.21	0.33	0.46	0.43	0.45	0.03
% grass of total dry Fine fuel	0.16	0.47	-0.28	-0.27	0	-0.46	0.35	-0.33	-0.24	-0.15	-0.08	0.14
Total fine fuel (tonne ha^{-1})	-0.2	0.09	-0.04	-0.26	0.28	-0.05	0.31	-0.21	0.14	-0.02	0.2	-0.14
Combustion completeness fine fuel (%)	0.31	0.65	-0.59	0.17	-0.38	-0.67	0.58	-0.07	-0.5	-0.6	-0.41	0.11
Combustion completeness coarse fuel (%)	0.07	0.01	-0.16	0.25	-0.15	-0.13	0.03	0.18	-0.25	-0.29	-0.27	-0.01
Combustion completeness heavy fuel (%)	0.13	0.32	-0.24	0.12	-0.16	-0.35	0.11	0.11	-0.24	-0.26	-0.26	0.01
Char height (cm)	0.04	0.22	-0.25	0.1	-0.02	-0.18	0.38	0.03	-0.24	-0.35	-0.11	0
Scorch height (cm)	-0.03	0.1	-0.29	0.47	-0.1	-0.11	0.35	0.36	-0.22	-0.39	-0.13	-0.07
Patchiness (Surface percentage burned)	-0.35	-0.22	0.28	-0.33	0.44	0.33	-0.02	-0.22	0.31	0.27	0.44	-0.16
Nitrogent to Carbon (ratio)	-0.15	-0.4	0.18	0.29	-0.1	0.36	-0.45	0.39	0.18	0.08	-0.08	-0.18
nitrogen content grass	0.29	0.19	-0.36	0.55	-0.35	-0.28	-0.08	0.58	-0.32	-0.38	-0.59	0.09
carbon content grass	0.09	-0.13	-0.1	0.61	-0.4	-0.01	-0.18	0.54	-0.08	-0.2	-0.36	-0.09
nitrogen litter grass	-0.1	-0.36	0.15	0.24	-0.22	0.39	-0.43	0.22	0.26	0.1	0.08	-0.18
carbon content litter	-0.09	0.11	-0.09	-0.05	-0.3	-0.12	-0.12	-0.16	-0.08	-0.07	-0.12	-0.23
average Carbon content	-0.04	-0.16	0.03	0.38	-0.26	0.05	-0.2	0.36	0.01	-0.03	-0.2	-0.15
average Nitrogen content	-0.12	-0.38	0.17	0.38	-0.12	0.32	-0.42	0.48	0.17	0.09	-0.09	-0.16

	pre-fire NDVI (MODIS)	dNDVI (MODIS)	dNBR (MODIS)	Pgreen (MODIS)	Fire weather index (ERA5)	Build up index (ERA5)	initial spread index (ERA5)	Fine fuel moisture code (ERA5)	FPAR (%) (MODIS)	LAI (MODIS)	LAI high vegetation (ERA5-land)	LAI low vegetation (ERA5-land)
Temperature (°C) Drone	-0.2	0.06	0.13	-0.26	0.12	0.06	0.19	0.2	-0.12	0.01	0.16	-0.04
Rel Humidity (%) Drone	0.37	0.03	-0.29	-0.18	-0.61	-0.6	-0.17	-0.64	0.52	0.47	0.45	0.46
Fuel moisture content (%)	0.07	0.01	-0.18	0.19	-0.17	-0.17	-0.11	-0.25	0.01	-0.09	-0	-0.02
Trees per hectacte	0.27	-0.04	0.04	-0.38	-0.43	-0.43	-0.06	-0.41	0.52	0.52	0.4	0.57
Average tree height (m)	0.4	0.07	-0.05	-0.03	-0.38	-0.36	0.09	-0.36	0.5	0.42	0.37	0.51
% grass of total dry Fine fuel	0.06	0.14	-0.31	0.06	0.14	0.14	-0.34	0.03	-0.12	-0.16	-0.18	-0.21
Total fine fuel (tonne ha^{-1})	-0.07	-0.07	0.04	-0.13	0.02	0.02	-0.31	-0.08	0.04	0.09	0.07	-0.1
Combustion completeness fine fuel (%)	-0.36	-0.01	-0.01	0.02	0.72	0.71	0.01	0.61	-0.62	-0.56	-0.6	-0.65
Combustion completeness coarse fuel (%)	-0.34	-0.11	0.18	-0.14	0.38	0.36	0.34	0.39	-0.32	-0.24	-0.15	-0.33
Combustion completeness heavy fuel (%)	-0.23	0.04	0.27	-0.02	0.33	0.31	0.14	0.39	-0.4	-0.29	-0.37	-0.42
Char height (cm)	-0.22	-0.01	0.18	-0.14	0.37	0.33	-0.03	0.3	-0.19	-0.16	-0.12	-0.42
Scorch height (cm)	-0.1	0.02	-0.03	-0.12	0.53	0.5	0.29	0.48	-0.16	-0.12	-0.2	-0.5
Patchiness (Surface percentage burned)	0.12	0.15	-0.03	-0.43	-0.2	-0.23	-0.3	-0.19	0.26	0.34	0.42	0.22
Nitrogent to Carbon (ratio)	0.18	-0.07	0.17	0.24	-0.15	-0.13	0.45	-0.01	0.19	0.16	0.02	0.17
nitrogen content grass	0.01	-0.06	0.02	0.44	0.26	0.24	0.63	0.29	-0.18	-0.26	-0.42	-0.32
carbon content grass	0.08	0.06	0.12	0.34	0.26	0.26	0.67	0.37	-0.15	-0.14	-0.34	-0.13
nitrogen litter grass	0.26	0.02	0.15	0.37	-0.11	-0.08	0.24	0.09	0.22	0.21	0.05	0.22
carbon content litter	-0.25	-0.06	0.25	0.11	0.14	0.16	0.11	0.22	-0.31	-0.22	-0.12	-0.01
average Carbon content	-0.15	-0.13	0.3	0.14	0.1	0.1	0.51	0.2	-0.15	-0.11	-0.15	0
average Nitrogen content	0.12	-0.05	0.21	0.2	-0.11	-0.1	0.53	0.03	0.15	0.15	0.03	0.16

5 **Figures**

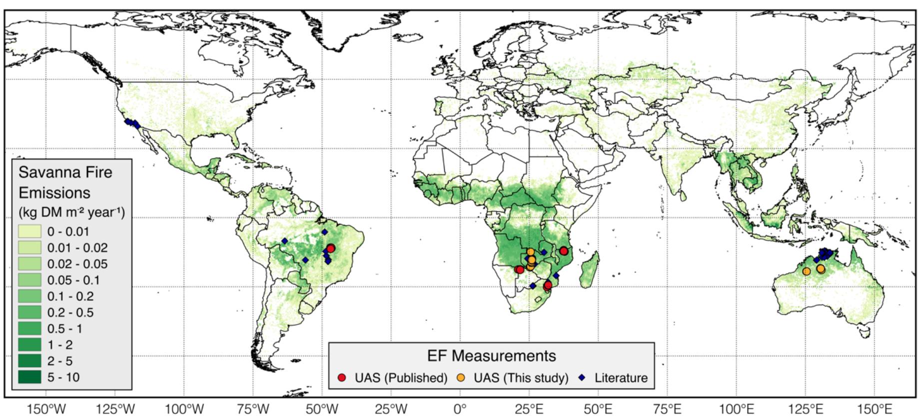

Figure 1. Overview of sampling locations used for the analysis. The previously published (red) and new (orange) UAS measurements as well as the locations of the included literature studies on savanna fire emission factors listed in Andreae, 2019 (yellow). The green shaded area shows the distribution of savanna and grassland fires over the 2002-2016 period according to GFED4s.

https://doi.org/10.5194/egusphere-2023-267
Preprint. Discussion started: 6 March 2023

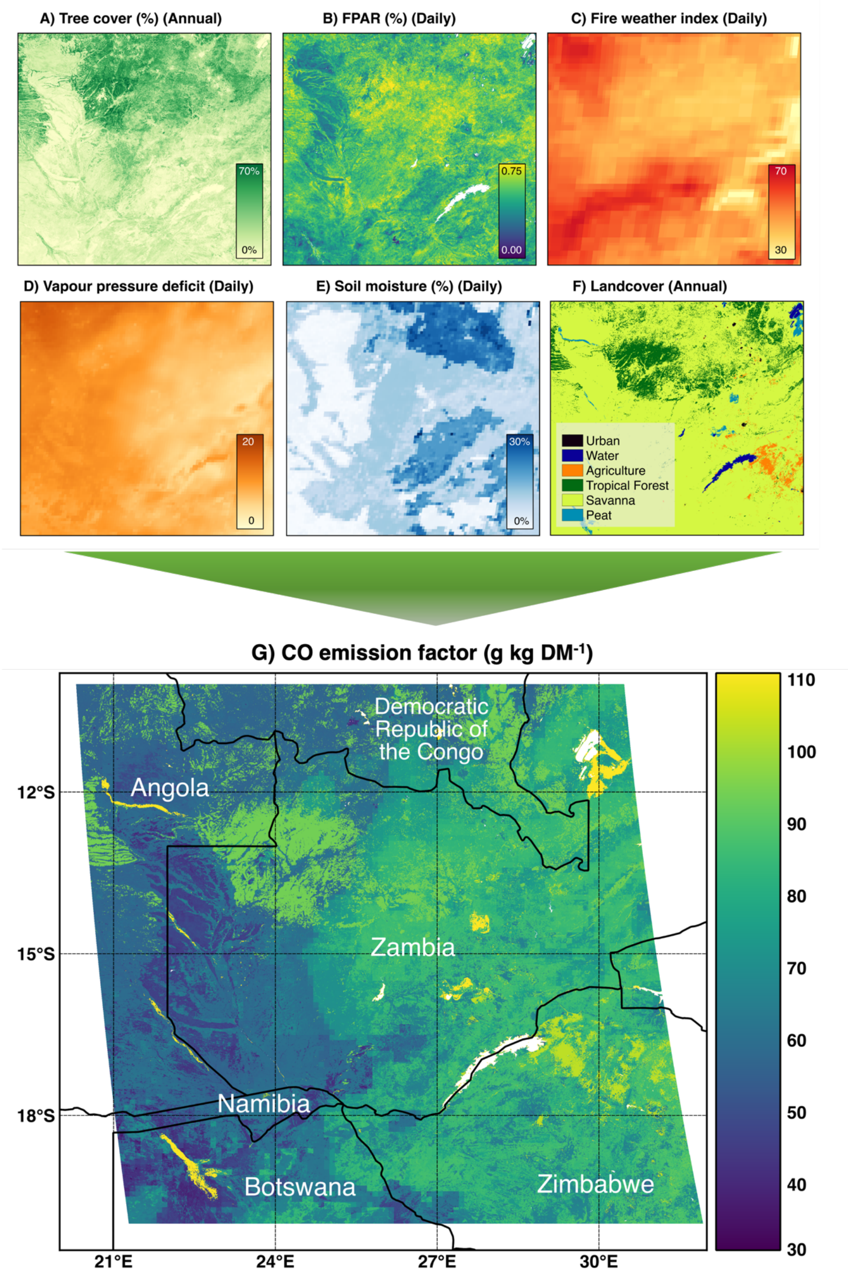

Figure 2: Estimation of the CO EF at 500-meter resolution for MODIS tile "h20v10" on June 1st, 2019 (g), using a random forest regression based on (a) fractional tree cover (FTC), (b) fraction of absorbed photosynthetically active radiation (FPAR), (c) the fire weather index (FWI), (d) vapour pressure deficit (VPD) and (e) soil moisture. For grid cells containing other biomes than savanna (f), GFED4s static EFs for the respective biome were imposed replacing the savanna EFs. Sources of the individual features are listed in Table 2.

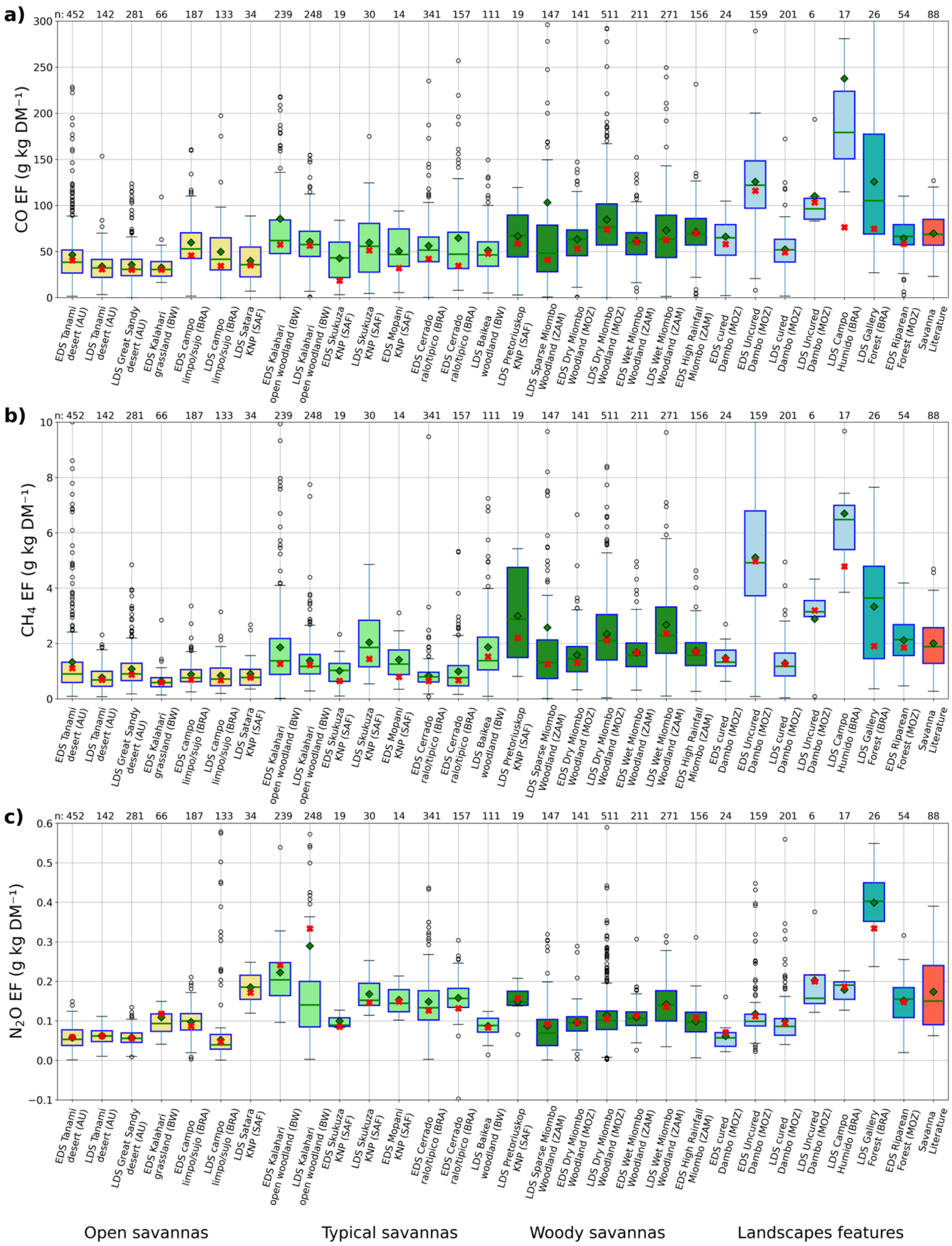

Figure 3: EFs (g kg DM^{-1}) measured in the sampled vegetation types during the EDS and LDS as well as the EFs from savanna measurements listed in savanna literature based on the Andreae (2019) compilation. The green diamond represents the arithmetic mean, and the red cross represents the EMR-weighted average value. The colours correspond to the savanna subclasses on the bottom of the figure. Table 1 lists the timeframes of the individual field campaigns while Table A1 in the appendix provides a broad floristic description of the dominant vegetation types.

https://doi.org/10.5194/egusphere-2023-267
Preprint. Discussion started: 6 March 2023

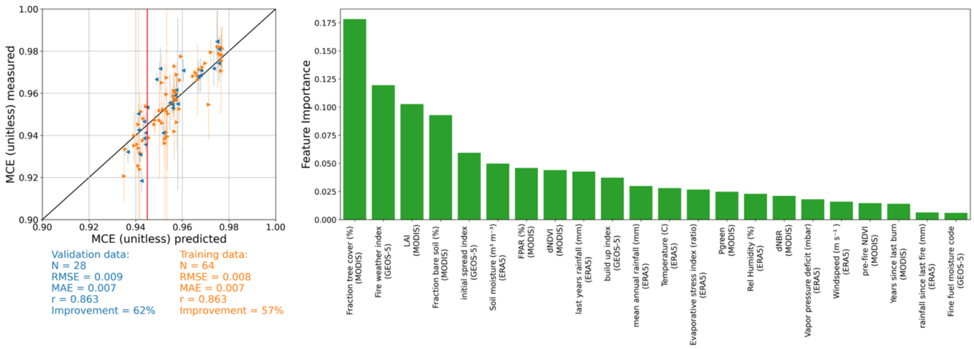

Figure 4. Left: Correlation of the predicted and measured fire-integrated weighted average MCE for the training (orange) and validation (blue) datasets. The vertical blue and orange lines represent the standard error of the mean within the respective fire. The red vertical line is the static MCE derived from the EFs used in GFED4s. The 'improvement' refers to the reduced mean absolute error compared to prediction using this static (red line) MCE. Right: The remote sensing and reanalysis datasets used by the model and the feature importance (an indication of how strong each feature is used to differentiate the data) of the respective features.

https://doi.org/10.5194/egusphere-2023-267
Preprint. Discussion started: 6 March 2023

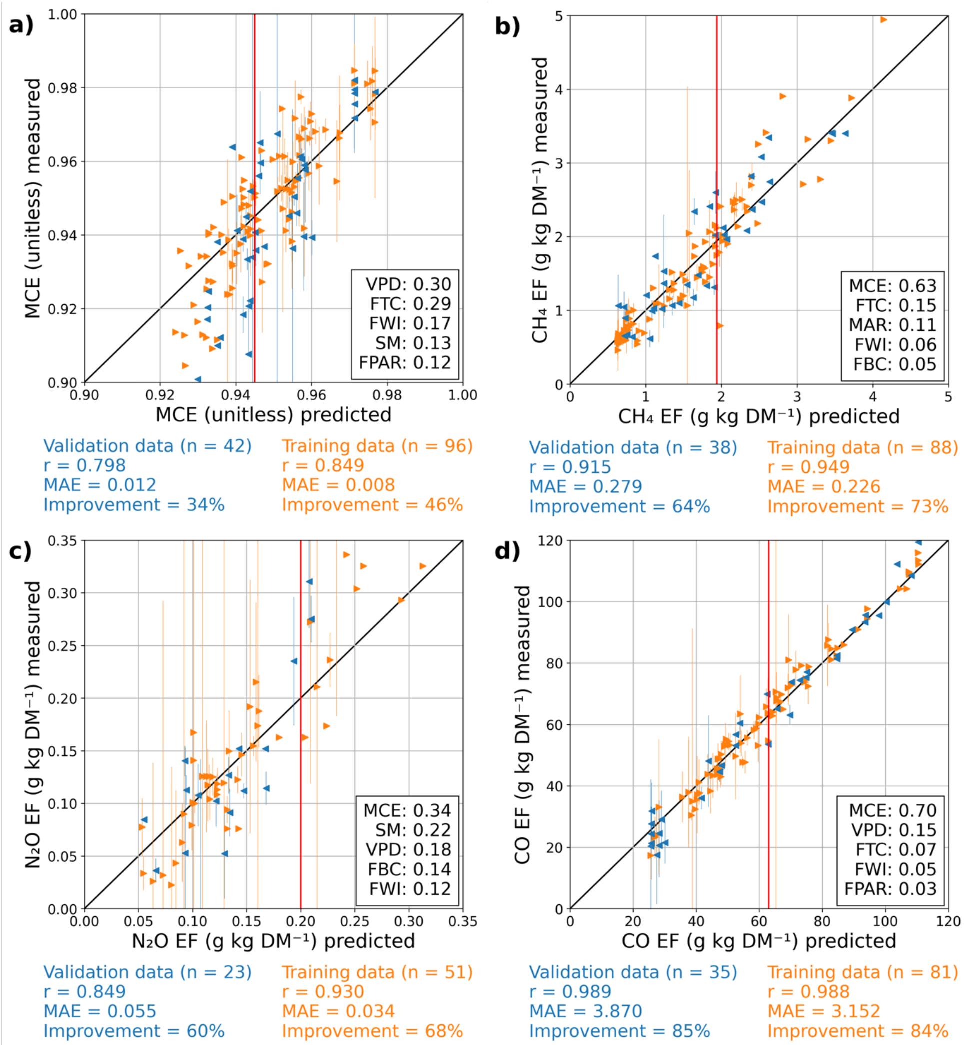

Figure 5. Pearson correlation of the predicted and measured fire-integrated WA MCE (a), CH_4 EF (b) N_2O EF (c), and CO EF (d) for the training (orange) and validation (blue) datasets using a limited set of features. The boxes in the bottom right of the panels list the remote sensing and reanalysis datasets used by the model and the feature importance (an indication of how strong each feature is used to differentiate the data). The red line represents the static biome-average used in GFED4s and 'improvement' refers to the reduced mean absolute error compared to this static average.

https://doi.org/10.5194/egusphere-2023-267
Preprint. Discussion started: 6 March 2023

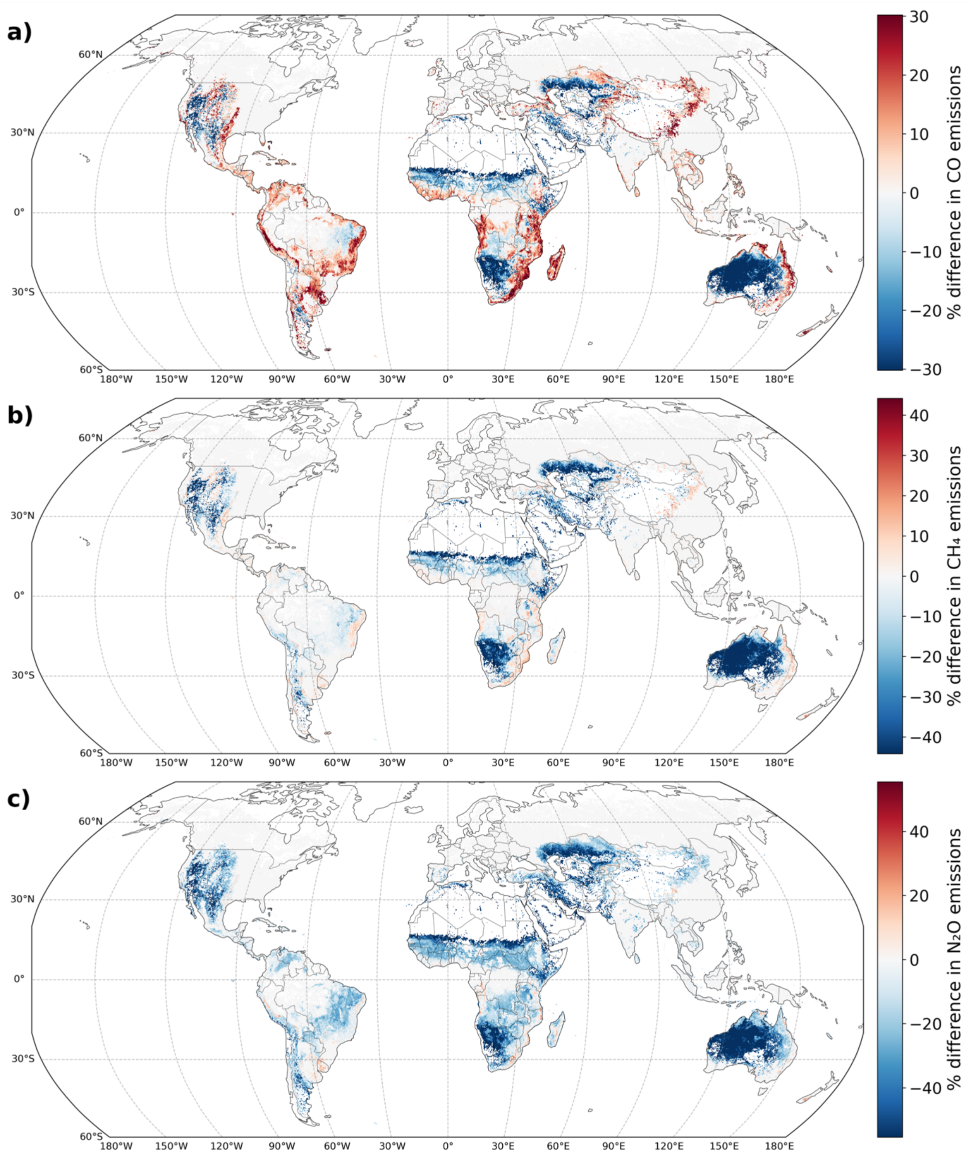

Figure 6: Difference in savanna and grassland fire emissions for CO (a), CH_4 (b) and N_2O (c) between emission computation using dynamic EFs versus static biome reference EFs (dynamic minus static), calculated using GFED4s for the 2002-2016 period.

https://doi.org/10.5194/egusphere-2023-267
Preprint. Discussion started: 6 March 2023

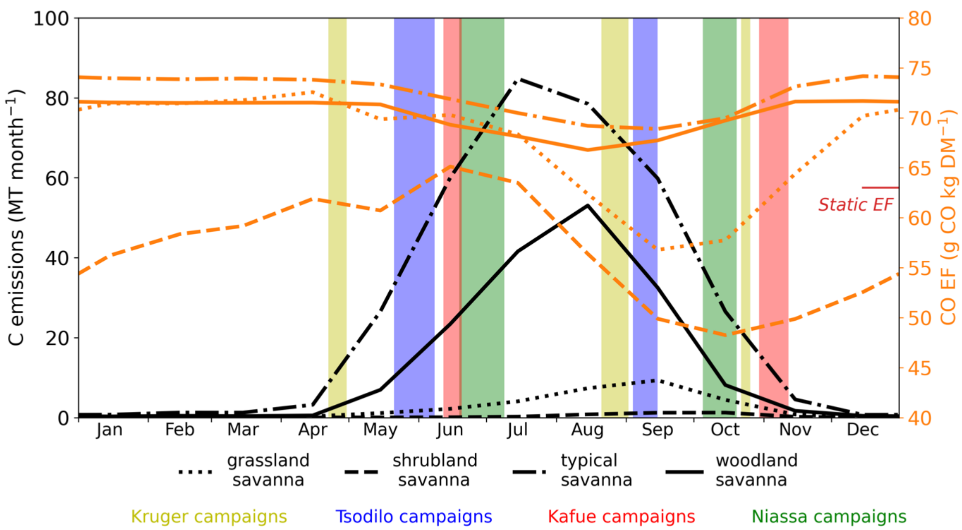

Figure 7. Seasonality of fire carbon emissions (black) and the computed CO EF (orange) for different savanna subclasses in southern hemisphere Africa, averaged over the 2002-2016 period. The savanna classes are based on the International Geosphere-Biosphere Program (IGBP) classification (Loveland and Belward, 1997). The shaded areas represent the timing of our measurements in southern hemisphere African savannas, indicating that especially our LDS campaigns may not be representative for the bulk of the fires. The red horizontal bar on the right represents the static EF used for savannas by GFED4s.

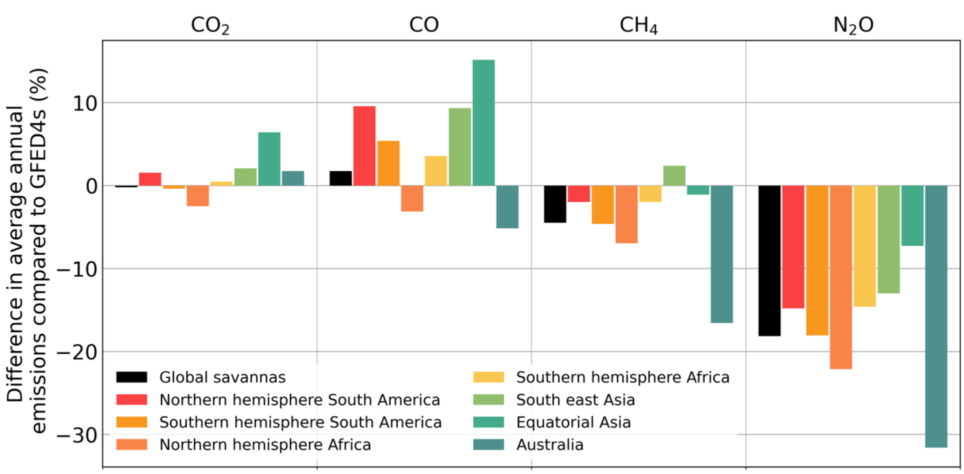

Figure 8: Relative difference in the landscape fire emissions of CO_2, CO, CH_4 and N_2O for the 2002-2016 period when using dynamic EFs versus static EFs using GFED4s (dynamic minus static) over the different savanna-rich GFED regions. Note that many of these regions encompass both xeric and mesic savannas with contrasting patterns that balance each other out. On a regional scale differences may therefore be much larger.

https://doi.org/10.5194/egusphere-2023-267
Preprint. Discussion started: 6 March 2023

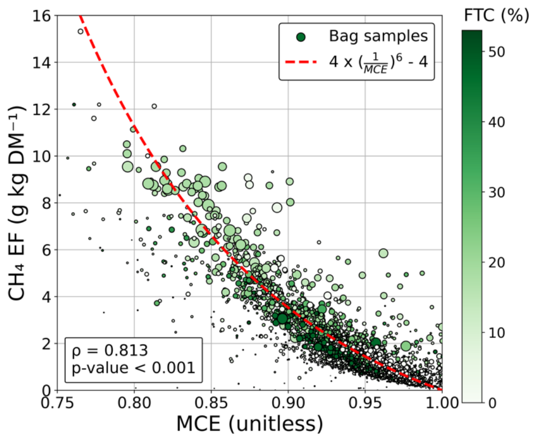

Figure 9. The non-linear regression between the CH_4 EF and the MCE for the individual bag samples. In the box on the bottom left, ρ refers to Spearman's rank correlation coefficient.

Appendix

Table A1: Floristic and geomorphological description of the different vegetation types measured in this study.

Vegetation type (Fig. 3)	Vegetation description[1,2]	Satellite value range in the plots
Dambo grasslands Niassa Special reserve, Mozambique	Landscape feature limited to more humid and fertile places, containing seasonally inundated grassland savanna dominated by perennial tussock grasses e.g. beard grass (*Andropogon (**PE**)*) and thatching grass (*Hyparrhenia (**A**)*) with sparse Bushwillow (*Combretum* (***D***)) trees and on clayey swales with highly variably water tables based on geomorphology and soil type (Mbanze et al. 2019).	MAR: 1000–1100mm FTC: 10 – 20% FBC: 10 – 30%
Dry Miombo woodlands Niassa Special reserve, Mozambique	Dry Miombo Woodland dominated by (5-15m) Semi-deciduous Miombo (*Brachystegia (**SD**)*) and Mnondo (*Julbernardia (**D**)*) trees on sandy soils (Ribeiro et al., 2013, 2008).	MAR: 850 – 1100mm FTC: 15 – 30% FBC: 10 – 25%
Wet Miombo woodlands, Kafue National Park, Zambia	Savanna open forest dominated by (5-15m) *Brachystegia (**SD**))*, *Julbernardia (**D**)*, and *Isoberlinia (**D**)* trees on sandy soils.	MAR: 850 – 1300mm FTC: 10 – 35% FBC: 0 – 10%
Sparse Miombo Woodlands, Bovu Forest reserve, Zambia	Savanna open woodland containing perennial tussock grasses e.g. digitgrass *(Digitaria (**PE**))* and Tangleheads (*Heteropogon (**A**)*) with (5-15m) *Combretum (**D**)*, *Albizia (**D**)* and *Diospyros (**EG**)* trees on sandy soils.	MAR: 800 – 900mm FTC: 5 – 15% FBC: 0 – 15%
Baikea woodland, Kasane Extension Forest Reserve, Botswana	Open woodland savanna dominated by tussock perennial grasses e.g. digitgrass (*Digitaria eriantha (**PE**)*) and sickle grass (*Pogonarthria squarrosa(**PE**)*) with scattered (5–15m) African teak (*Baikiaea plurijuga (**D**)*) and silver cluster-leaf (*Terminalia sericea (**D**)*) trees on sandy soils.	MAR: 700 – 800mm FTC: 5 – 10% FBC: 5 – 20%
Satara experimental burn plots, Kruger National Park, South Africa	Grassland savanna dominated by perennial tussock grasses e.g. Sabi grass (*Urochloa mosambicensis (**PE**)*) and digitgrass (*Digitaria eriantha (**PE**)*) with scattered tall (10–15m) Marula (*Sclerocarya birrea (**D**)*) and knobthorn Acacia (*Acacia*	MAR: 400 – 550mm FTC: 0 – 5% FBC: 10 – 30%

https://doi.org/10.5194/egusphere-2023-267
Preprint. Discussion started: 6 March 2023

	nigrescens ***(D)***) trees on clay soils overlying basalt plains (Venter and Govender, 2012).	
Skukuza experimental burn plots, Kruger National Park, South Africa	Savanna woodland dominated by dense Bushwillow (*Combretum collinum* ***(D)****/ Combretum zeyheri* ***(D)****)* trees on hydromorphic or duplex soils containing granite outcrops (Venter and Govender, 2012).	MAR: 500 – 600mm FTC: 3 – 10% FBC: 25 – 30%
Mopani experimental burn plots, Kruger National Park, South Africa	Savanna shrubland dominated by dense low (1–4m) mopane (*Colophospermum mopane* ***(D)***) shrubs on flat or slightly sloping clay soils. (Venter and Govender, 2012).	MAR: 300 – 450mm FTC: 0 – 10% FBC: 30 – 50%
Pretoriuskop experimental burn plots, Kruger National Park, South Africa	Open forest savanna dominated by dense tall (10–15m) clusterleaf (*Terminalia sericea* ***(D)***) and (5-10m) Sicklebush (*Dichrostachys cinerea* ***(SD)***) trees on sandy soils. (Venter and Govender, 2012).	MAR: 800 – 900mm FTC: 0 – 20% FBC: 5 – 15%
Mata galleria, EESGT, Brazil	Riparian forest lining rivers dominated by palm trees e.g. *Mauritia flexuosa* with an undergrowth of perennial grasses e.g. bahiagrass (*paspalum veredense* ***(PE)***) and *Abolboda poarchon* ***(PE)*** on gleysols that remain very humid for most of the year.	MAR: 1400–1500mm FTC: 20 – 50% FBC: 20 – 25%
Campo humido, Estação Ecológica Serra Geral do Tocantins, Brazil	Seasonally inundated grasslands dominated by perennial grasses e.g. bahiagrass (*paspalum veredense* ***(PE)***) and carpet grass *(axonopus canescens* ***(PE)****)* with sparse palm trees (*Mauritia flexuosa*) on gleysols that remain humid for most of the year.	MAR: 1400–1500mm FTC: 5 – 10% FBC: 20 – 25%
Campo limpo/ sujo, Estação Ecológica Serra Geral do Tocantins, Brazil	Grassland savannas dominated by perennial tussock grasses e.g. carpet grass (*Axonopus* ***(PE)***, bluestems (*Schizachyrium* ***(PE)*** and Crinkleawn grass *(Trachypogon* ***(PE)*** on sandy soils.	MAR: 1300–1500mm FTC: 0 – 5% FBC:10 – 50%
Cerrado ralo/ Cerrado tipico, Estação Ecológica Serra Geral do Tocantins, Brazil	Open woodland savanna dominated by perennial tussock grasses e.g. carpet (*Axonopus* ***(PE)***, bluestems (*Schizachyrium* ***(PE)*** and Crinkleawn grass *(Trachypogon* ***(PE)*** with sparse overgrowth of *pigeonwood (Hirtella ciliate* ***(SD)****), earringwood (Rourea induta* ***(SD)****)* trees on deep sandy soils.	MAR: 1300–1500mm FTC: 0 – 10% FBC:10 – 60%
Kalahari open woodland, NW Ngamiland, Botswana	Open woodland savanna dominated by tussock perennial grasses e.g. digitgrass (*Digitaria eriantha* ***(PE)***) and sickle grass (*Pogonarthria squarrosa* ***(PE)***) with scattered (5–15m) African teak (*Baikiaea plurijuga* ***(D)***) and silver cluster-leaf (*Terminalia sericea* ***(D)***) trees on sandy hills.	MAR: 650 – 750mm FTC: 0 – 5% FBC: 20 – 35%
Kalahari grassland, NW Ngamiland, Botswana	Open grassland savanna dominated by tussock perennial e.g. *Stipagrostis uniplumis* ***(PE)*** and *Eragrostis rigidior* ***(PE)*** on clay soils.	MAR: 700 – 750mm FTC: 0 – 2% FBC: 25 – 30%
Great sandy desert, Ngurrara country, Western Australia	Grasslands dominated by spinifex hummocks (*Triodia* ***(PE)***) interspersed with open (5–10m) semi-evergreen *Eucalypt* ***(SE)*** woodlands and *Acacia* ***(D)*** shrubs on lateritic swales and red sand dunes.	MAR: 400 – 450mm FTC: 0 – 1% FBC: 65 – 90%
Tanami desert, Warlpiri country, Northern Territory, Australia	Hummock-grass (*Triodia spinifex* ***(PE)***) dominated grasslands interspersed with open (5–10m) semi-evergreen *Eucalypt* ***(SE)*** woodlands and *Acacia* ***(D)*** shrubs on sand plains.	MAR: 500 – 600mm FTC: 1 – 3% FBC: 50 – 85%

[1] life cycle of the dominant grass species; **PE**: perennial > 2 years; **AN**: Annual grasses
[2] Deciduousness of the dominant trees; **D**: Deciduous, **SD**: Semi-deciduous, **EG**: Evergreen